Calhoun
Institutional Archive of the Naval Postgraduate School

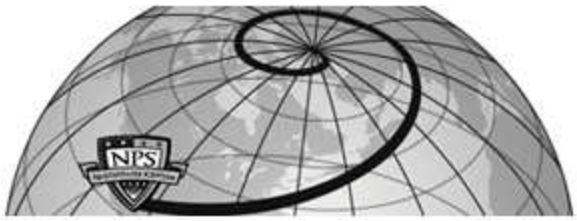

Author(s)	Myrick, Kenneth B.
Title	Coastal bathymetry using satellite observation in support of intelligence preparation of the environment
Publisher	Monterey, California. Naval Postgraduate School
Issue Date	2011-09
URL	http://hdl.handle.net/10945/5519

This document was downloaded on May 04, 2015 at 23:14:28

DUDLEY KNOX LIBRARY

http://www.nps.edu/library

Calhoun is a project of the Dudley Knox Library at NPS, furthering the precepts and goals of open government and government transparency. All information contained herein has been approved for release by the NPS Public Affairs Officer.

Dudley Knox Library / Naval Postgraduate School
411 Dyer Road / 1 University Circle
Monterey, California USA 93943

NPS PRAESTANTIA PER SCIENTIAM 1909

http://www.nps.edu/

NAVAL POSTGRADUATE SCHOOL

MONTEREY, CALIFORNIA

THESIS

COASTAL BATHYMETRY USING SATELLITE OBSERVATION IN SUPPORT OF INTELLIGENCE PREPARATION OF THE ENVIRONMENT

by

Kenneth B. Myrick II

September 2011

Thesis Advisor:	Richard C. Olsen
Second Reader:	Jamie MacMahan

Approved for public release; distribution is unlimited

THIS PAGE INTENTIONALLY LEFT BLANK

REPORT DOCUMENTATION PAGE			Form Approved OMB No. 0704-0188
Public reporting burden for this collection of information is estimated to average 1 hour per response, including the time for reviewing instruction, searching existing data sources, gathering and maintaining the data needed, and completing and reviewing the collection of information. Send comments regarding this burden estimate or any other aspect of this collection of information, including suggestions for reducing this burden, to Washington headquarters Services, Directorate for Information Operations and Reports, 1215 Jefferson Davis Highway, Suite 1204, Arlington, VA 22202-4302, and to the Office of Management and Budget, Paperwork Reduction Project (0704-0188), Washington, DC 20503.			
1. AGENCY USE ONLY *(Leave blank)*	**2. REPORT DATE** September 2011	**3. REPORT TYPE AND DATES COVERED** Master's Thesis	
4. TITLE AND SUBTITLE Coastal Bathymetry Using Satellite Observation in Support of Intelligence Preparation of the Environment			**5. FUNDING NUMBERS**
6. AUTHOR(S) Kenneth B. Myrick II			
7. PERFORMING ORGANIZATION NAME(S) AND ADDRESS(ES) Naval Postgraduate School Monterey, CA 93943-5000			**8. PERFORMING ORGANIZATION REPORT NUMBER**
9. SPONSORING /MONITORING AGENCY NAME(S) AND ADDRESS(ES) N/A			**10. SPONSORING/MONITORING AGENCY REPORT NUMBER**
11. SUPPLEMENTARY NOTES The views expressed in this thesis are those of the author and do not reflect the official policy or position of the Department of Defense or the U.S. Government. IRB Protocol number NA.			
12a. DISTRIBUTION / AVAILABILITY STATEMENT Approved for public release; distribution is unlimited			**12b. DISTRIBUTION CODE**

13. ABSTRACT (maximum 200 words)

Subaqueous beach profiles are obtained for littoral regions near Camp Pendleton, CA, using observations of wave motion. Imagery was acquired from WorldView2 Satellite on 24 March 2010. Two sequential images taken 10 seconds apart are used for the analyses herein. Water depths were calculated using linear dispersion relationship for surface gravity waves. Depth profiles were established from shoreline out to 1 kilometer offshore and depths of up to 15 meters. Comparisons with USGS DEM values show agreement within five percent in the surf zone (shoreline to wave breaking) and one percent outside the surf zone (offshore of wave breaking).

14. SUBJECT TERMS Remote Sensing, Multispectral, 8-Color, Bathymetry, World View-2, ENVI, Principal Component Transform, Depth Inversion, Wave Methods, Dispersion Relation, IPE, Intelligence Preparation of the Environment.			**15. NUMBER OF PAGES** 75
			16. PRICE CODE
17. SECURITY CLASSIFICATION OF REPORT Unclassified	**18. SECURITY CLASSIFICATION OF THIS PAGE** Unclassified	**19. SECURITY CLASSIFICATION OF ABSTRACT** Unclassified	**20. LIMITATION OF ABSTRACT** UU

NSN 7540-01-280-5500

Standard Form 298 (Rev. 2-89)
Prescribed by ANSI Std. 239-18

THIS PAGE INTENTIONALLY LEFT BLANK

Approved for public release; distribution is unlimited

COASTAL BATHYMETRY USING SATELLITE OBSERVATION IN SUPPORT OF INTELLIGENCE PREPARATION OF THE ENVIRONMENT

Kenneth B. Myrick II
Lieutenant Commander, United States Navy
B.S., Thomas A. Edison State College, 2000

Submitted in partial fulfillment of the
requirements for the degree of

MASTER OF SCIENCE IN SPACE SYSTEMS OPERATIONS

from the

NAVAL POSTGRADUATE SCHOOL
September 2011

Author: Kenneth B. Myrick II

Approved by: Dr. Richard C. Olsen
Thesis Advisor

Dr. Jamie MacMahan
Second Reader

Dr. Rudy Panholzer
Chair, Space Systems Academic Group

THIS PAGE INTENTIONALLY LEFT BLANK

ABSTRACT

Subaqueous beach profiles are obtained for littoral regions near Camp Pendleton, CA, using observations of wave motion. Imagery was acquired from WorldView2 Satellite on 24 March 2010. Two sequential images taken 10 seconds apart are used for the analyses herein. Water depths were calculated using linear dispersion relationship for surface gravity waves. Depth profiles were established from shoreline out to 1 kilometer offshore and depths of up to 15 meters. Comparisons with USGS DEM values show agreement within five percent in the surf zone (shoreline to wave breaking) and one percent outside the surf zone (offshore of wave breaking).

THIS PAGE INTENTIONALLY LEFT BLANK

TABLE OF CONTENTS

LIST OF FIGURES

LIST OF TABLES

THIS PAGE INTENTIONALLY LEFT BLANK

LIST OF ACRONYMS AND ABBREVIATIONS

AGI	Analytical Graphics Inc.
ANFIS	Adaptive-Network-based Fuzzy Inference System
CEOF	Complex Empirical Orthogonal Function
CRAB	Coastal Research Amphibious Buggy
DEM	Digital Elevation Model
ENVI	Environment for Visualizing Images
HADR	Humanitarian and Disaster Relief
IfSAR	Interferometric Synthetic Aperture Radar
IPE	Intelligence Preparation of the Environment
LEO	Low Earth Orbit
LIDAR	Light Detection and Ranging
RST	Resampling, Scaling, and Translation
SNR	Signal to Noise Ration
SONAR	Sound Navigation and Ranging
STK	Satellite Tool Kit
UAV	Unmanned Aerial Vehicle
USGS	United States Geological Survey

THIS PAGE INTENTIONALLY LEFT BLANK

ACKNOWLEDGMENTS

I would like to thank Dr. Richard C. Olsen and Dr. Jamie MacMahan for their guidance and support during the development of this thesis. Additionally, I would like to thank Ms. Angela Kim and Ms. Krista Lee for their tremendous support and encouragement throughout this process. Their encouragement was invaluable and very much appreciated.

Furthermore, I would like to thank Major Frank Harmon for continually providing me with the motivation I needed to complete this thesis. I would also like to give a special thanks to his loving wife Ms. Cariann Colman, for her support, encouragement, motivation, and providing me with nourishing home-cooked meals in the absence of my family during the last three months of this process.

Finally, I would like to thank my loving wife, Patsy, and our two boys, Dusty and Dakota, for their love, support, encouragement, and understanding. They are my life, and without them none of this would have been possible.

THIS PAGE INTENTIONALLY LEFT BLANK

I. INTRODUCTION

A. PURPOSE OF RESEARCH

Nearshore bathymetry is used for Intelligence Preparation of the Environment (IPE) in support of amphibious operations, Humanitarian and Disaster Relief (HADR), and mine warfare planning operations. "The Navy, in support of amphibious operations, also requires the ability to remotely and surreptitiously determine the bathymetry profile of the ocean near amphibious landing zones" (OPNAV N2/N6, 2010). In most instances, IPE will be conducted in denied areas where it is not feasible or in many instances possible for platforms to gain the required access to conduct bathymetry determination from the standard Navy operational tools such as Light Detection and Ranging (LIDAR) or Sound Navigation and Ranging (SONAR). Although bathymetry can be measured through various means, satellites from Low Earth Orbit (LEO) can safely transit over denied territories to produce nearshore subaqueous beach profiles. The wave celerity method using the linear dispersion relationship for surface gravity waves is a convenient method to accurately estimate nearshore subaqueous beach profiles from satellite imagery.

Estimating water depth from aerial photography by the linear dispersion relation for surface gravity waves is not a new technique. In fact, a very similar method for determining the bathymetry off hostile beaches was used during both World War I and World War II (Caruthers, Arnone, Howard, Haney, & Durham, 1985; Williams, 1947). However, due to cost and a number of significant limitations affecting the accuracy, once the stress of war and need to access denied coastal areas was removed the Navy stopped using it as a peace time tool (Williams, 1947).

The purpose of this thesis is to show that determining nearshore bathymetry from multispectral satellite imagery is a viable and accurate method in support of IPE. If shallow water wave celerity or wave length can be determined from satellite imagery, then water depth can be calculated by the linear dispersion relation for surface gravity waves. This thesis will show that, by taking advantage of the different characteristics of

multispectral imagery, wave crest can be clearly resolved allowing for the determination of both wave celerities and wave lengths. In addition, a number of the limitations associated with both methods of the linear dispersion relation for surface gravity waves to estimate water depth can be minimized resulting in sufficiently detailed and accurate depth determination for the purpose of IPE in support of amphibious operations, HADR, and mine warfare planning.

B. SPECIFIC OBJECTIVES

For the purpose of this study, ten WorldView-2 multispectral images were taken in rapid succession at approximately ten second intervals of Camp Pendleton, California. The imagery was processed with Environment for Visualizing Images (ENVI) software to register the images, identify wave crest, measure wave lengths, and determine wave celerity. Depth was estimated at approximately eighty locations by applying the linear dispersion relation for surface gravity waves, by the celerity method, to the data derived from the imagery processing. Next, these estimated depths were compared to ground truth data as determined from a United States Geological Survey (USGS) Digital Elevation Model (DEM). Finally, this study demonstrates that applying the linear dispersion relation for surface gravity waves to wave data, determined from multispectral satellite electro-optical imagery, is a viable technique for determining bathymetry in denied or restricted areas in support of IPE.

II. BACKGROUND

A. HISTORY

1. Early Bathymetry of Denied Areas in Support of Military Operations

There are examples where the U.S. military has relied heavily on bathymetry determination of denied or hostile areas by remote sensing methods to ensure the success of military operations as far back as World War I. The coastal bathymetry off both the Beaches of Normandy and the beaches on the Flanders coast were determined with early remote sensing methods to ensure the success of those operations (Williams, 1947). During a time of hostilities leading up to these military operations it was not practical to conduct hydrographic surveys off the coast of these enemy held beaches. However, there were very important questions that needed to be answered to ensure the success of the operations and the accurate determination of coastal bathymetry held the answers to many of those questions. The importance of determining coastal bathymetry to answer questions like: "How far to seaward will craft ground? To what extent will it be necessary to waterproof the vehicles to be unloaded? What kind of craft should be used? Will special equipment such as pontoons be needed? Will men be in danger of drowning in deeper water inshore of where the craft ground?" (Williams, 1947) and determination of beach obstacles is obvious when landing forces on hostile beaches, and these same questions are still applicable today. In 1947, W.W. Williams outlined four ways to determine coastal bathymetry with remote sensing.

a. The Waterline Method

The Waterline Method was the method used for both Flanders and Normandy. In this method, bathymetry determination is made by drawing contours of the waterlines on aerial photographs taken of shorelines at carefully recorded times and then computing the tide height from the time record from the Admiralty Tables. This method was used throughout World War II for almost every amphibious operation due to its simplicity and ease to be operationalized (Williams, 1947).

This method has a number of significant limitations; however, the worst of which was the fact that it was useless for bathymetry below the low spring tide levels and had no application to tideless waters. Therefore, it was determined that some other method of obtaining coastal bathymetry was needed in order to calculate bathymetry out to at least two fathoms below mean low water-level (Williams, 1947).

b. The Transparency Method

In 1942, it was noted that in a photograph of a swimming pool the image density was greater in the deeper end than in the shallow end. Further investigation showed that photographs of beaches revealed the same phenomenon in the coastal waters but not always (Williams, 1947). The transparency method is based on the fact that light on the surface of the water is reflected, absorbed, transmitted, and scattered by varying amounts (Olsen, 2007). The light that is transmitted is reflected off of light colored sediments and is transmitted up through the water and toward the imaging sensor, in shallow water.

In 1943, this method was used to map the deep water channel in the Seine River below Rouen and was used qualitatively to locate sandbanks and shoals. However, this method suffers from numerous limitations that made it impractical to operationalize primarily due to the fact that "it is doubtful whether quantitatively the method can be of great value" (Williams, 1947). This is due to limitations, such as choppy seas, which increase scattering, resulting in the image coming from the water surface and not the seabed. Other serious limitations are suspension of particulates in the water that prevent light from transmitting through the entire water column, and dark plant and sediment materials on the seabed that increase absorption and decrease reflection of incident light. Both result in density of the photographic image not being a simple function of water depth. These serious limitations resulted in this method being determined as unreliable and dangerous for military operations and therefore was abandoned (Williams, 1947). This approach has since been revisited in several modern studies using modern technology and multispectral imagery, and is proving to be a practical method (Gao, 2009).

c. The Wave Celerity Method

The wave celerity method relies on the linear dispersion relationship between wave celerity, wave period, wave length, and water depth. The wave celerity and wave length are determined from successive images where the exact time between images and image scale are known. Figure 1 shows curves used to quickly determine water depth once wave length and wave celerity were known (Williams, 1947).

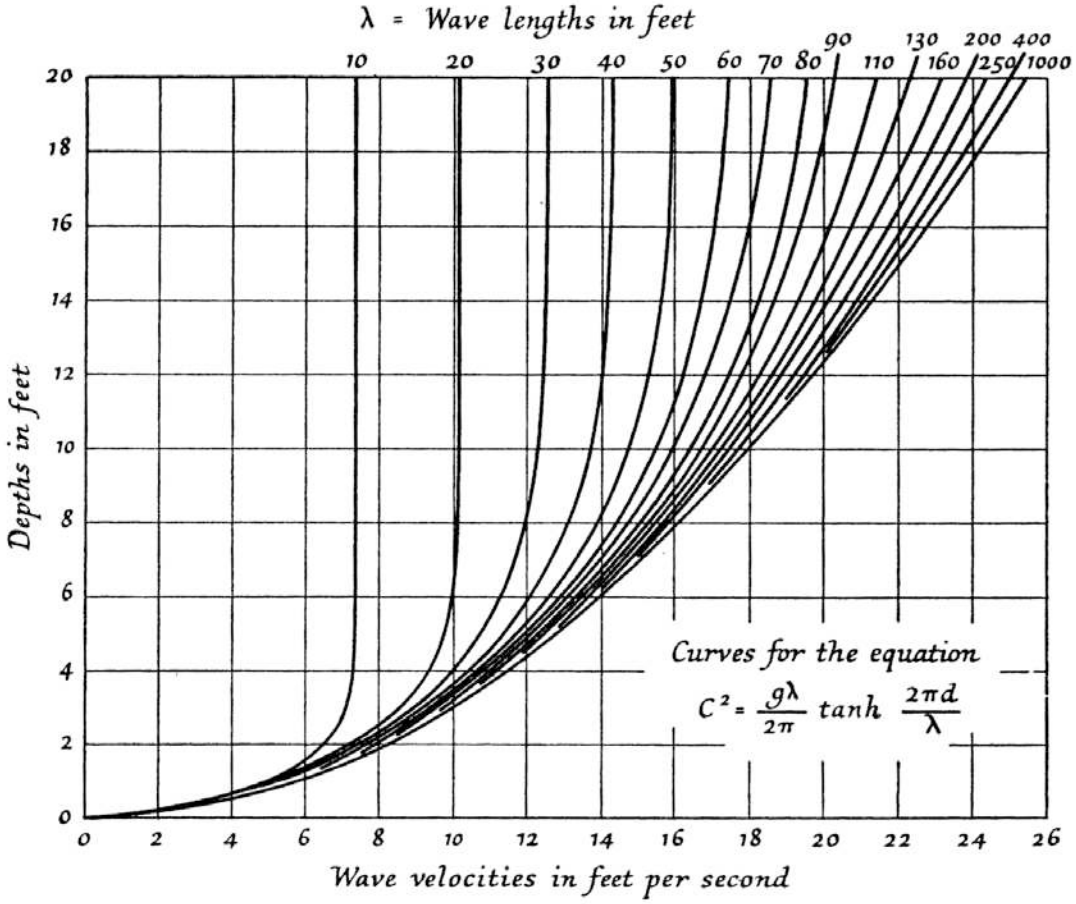

Figure 1. Curves relating water depth to wave length and celerity (From Williams, 1947)

The curves in Figure 1 show that waves with long wave lengths travel at faster speeds than those with shorter wave lengths. In addition, in deep water a wave's celerity is unaffected by depth, but as waves enter shallow water at depths less than their wave length they begin to feel the affect of the bottom. This results in a decrease in wave

celerity corresponding to the decrease in depth. This relation allows the expression of depth as a function of wave celerity, which will be discussed in more detail in Section B of this chapter (Williams, 1947).

In 1947, Williams noted that this method suffered from a number of issues to include accuracy of image acquisition times, scale and registration of images, and low image resolution (Williams, 1947). This method is very similar to the method explored in this thesis as the same math is valid, however, with the use of multispectral satellite imagery much of the afore mentioned uncertainties can easily be overcome.

d. The Wave Period Method

The wave period method was used in the absence of accurate clocks fitted to the cameras. The formula was adapted to establish a relationship between the wave period, the wave length, and the water depth. Then, curves were plotted for this new relationship to produce Figure 2 in order for wave period to be determined from a known depth and measured wave length from untimed photographs. Once the deep water wave period was determined from Figure 2, this period was used to calculate the wave celerity of shallow water waves again using measured wave length from untimed photographs (Williams, 1947).

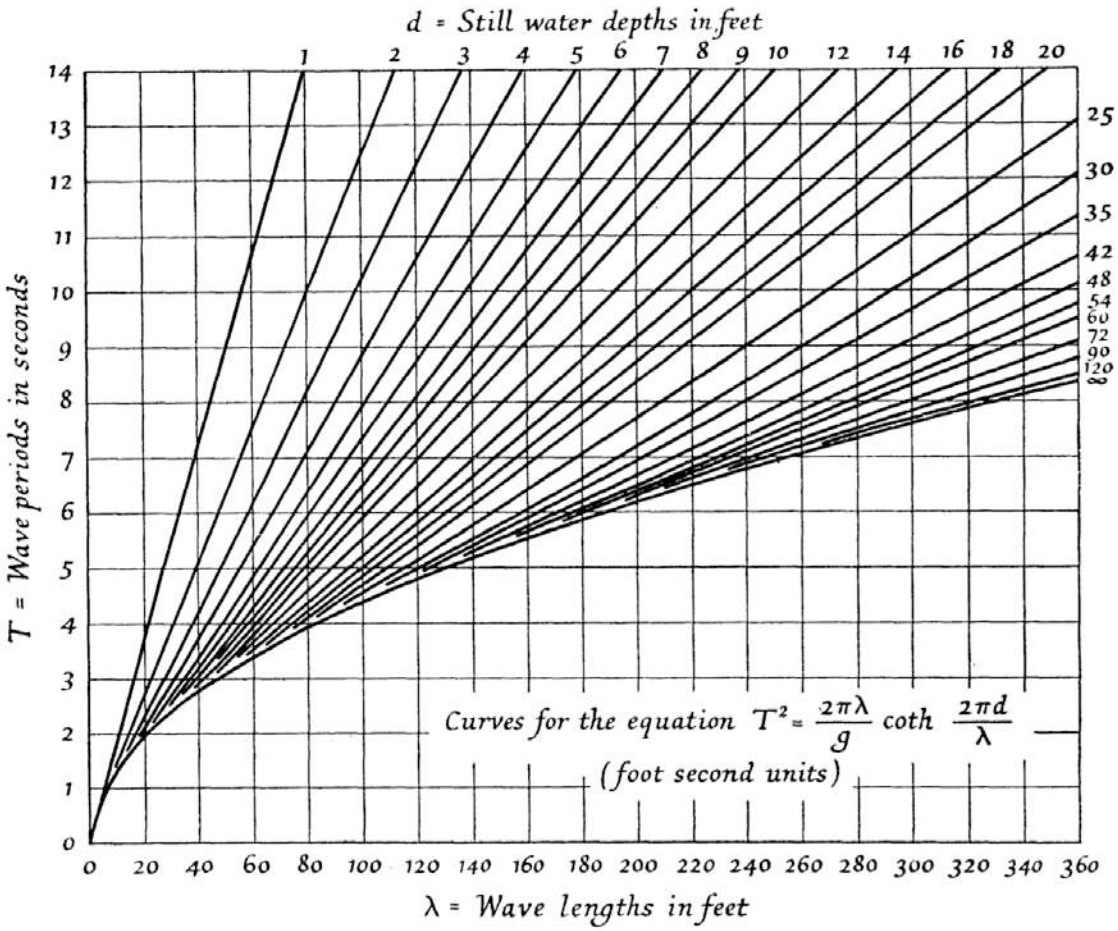

Figure 2. Curves relating wave period to depth and wave length (From Williams, 1947)

The correct determination of wave period is critical for this method as small inaccuracies in the wave period can cause large errors in depth determination. This results in a number of significant issues with this method. First, accurate deep water depths must be already known or able to be determined from accurate bathymetry charts. Secondly, to ensure the most accurate determination of wave period, waves at the deepest possible depth must be selected, which causes problems as deep water wave crest are not well defined and therefore hard to resolve and measure wave lengths from photographs (Williams, 1947). This method still suffers from the same issues making the wave celerity method the preferred method.

2. Operational Capability to Determine Nearshore Bathymetry

Methods that used the linear dispersion relationship, the wave period method and the wave celerity method, to determine nearshore bathymetry from photography were never truly developed into an operational capability after World War II. The Navy ceased using these methods, likely due to the fact that these methods were considered extremely expensive and suffered from limitations resulting in varying degrees of accuracy (Williams, 1947). This coupled with the fact that there was no longer a need to determine nearshore bathymetry of denied or inaccessible enemy beaches lead to the determination that they were not applicable for peace time operations (Williams, 1947).

In 1985, however, the Naval Ocean Research and Development Activity conducted a study to provide an operational capability to determine nearshore bathymetry for preamphibious assault planning. In this study, they revisited both the wave period method and the wave celerity method to determine their applicability as an operational capability to determine water depth from photography. This study concluded that these methods were not feasible as an operational capability for detailed accurate depth determination due to a number of significant problems and limitations discussed below (Caruthers et al., 1985).

a. Sunglint

The proper sunglint or sun angle conditions is required for wave pattern enhancements in order to recognize wave features to break out wave crest for proper measurement of wave lengths and wave celerity determination. "The use of sunglint accents wave features by imaging wave crests as bright tones and the troughs as dark tones in locations where the waves are perpendicular to the sun's rays" (Caruthers et al., 1985). For aerial photography, this requires that the flight tracks be coordinated with beach orientation and sun angle placing significant limitations on the collection method. Figure 3 shows both optimum wave detection and poor wave detection from sunglint (Caruthers et al., 1985).

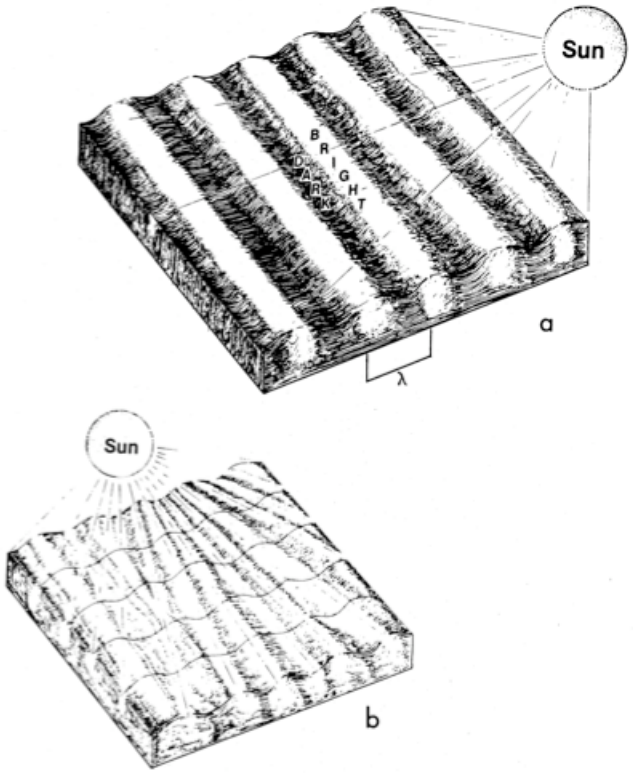

Figure 3. (a) Optimum wave detection: sun rays perpendicular to wave direction. (b) Poor wave detection: sun rays parallel to wave direction. (From Caruthers et al., 1985)

The need to plan and coordinate the flight track can be reduced by the use of satellite imagery, as modern imaging satellites have the ability to image well off nadir allowing the sun angle to be precisely optimized (Abileah, 2006).

b. Scale

Minimizing mensuration errors is crucial to ensuring accuracy of determining depths. In order to minimize the degree of error introduced by the scale of the photography, the proper scale for the mensuration method must be known. This placed significant limitations on not only mensuration methods and photography sources, but also idealized swell patterns (Caruthers et al., 1985). This limitation is minimized by digital multispectral satellite imagery and imagery processing software for mensuration.

Commercial satellite imagery can provide up to 50 cm resolution, significantly improving the ability to resolve wave features, thus minimizing the mensuration error. In addition, multispectral imagery allows for the removal of image contamination such as clouds, contrails, whitecaps, and ship wakes further improving the image quality and minimizing the mensuration error.

c. Bottom Slope Conditions

A basic assumption in applying the linear dispersion method is that a constant bottom slope exists. This is not always a valid assumption in coastal regions and can result in significant errors in depth determination. Gradients must be minimal over a given wave length for the linear dispersion method to provide accurate depth determination; otherwise errors in depth calculations can exceed thirty percent of actual depth (Caruthers et al., 1985).

3. Modern Studies to Determine Nearshore Bathymetry

There still exists today a need to develop an operational capability to determine nearshore bathymetry of denied or hostile coastal regions for IPE in support of amphibious operations, mine warfare, and HADR planning. Since 1985, there have been numerous studies conducted in an attempt to develop a more accurate method of determining nearshore bathymetry, and overcome the limitations associated with the wave celerity method from remote sensing platforms. The large majority of the studies conducted since 1985, still use the linear dispersion relationship for surface gravity waves for the actual depth determination, though they have varied the collection method and the parameters collected. This section will discuss a number of those methods.

a. X-Band Marine Radar

X-Band marine radars can be used to image the sea surface, and then the resulting "sea clutter" on the radar image sequences can be exploited to determine the two-dimensional wave spectra. A three-dimensional Fourier Transform analyses, on a sequence of radar images, maps wave celerity and direction. Wave period can also be determined from the radar data. Estimated depth is calculated by the linear dispersion

relationship from the wave celerity and wave period applying the same mathematical relationships as in the wave celerity method previously discussed. Figure 4 is a plot of wave celerity and direction determined with data from standard X-Band marine radar (Bell, 1999).

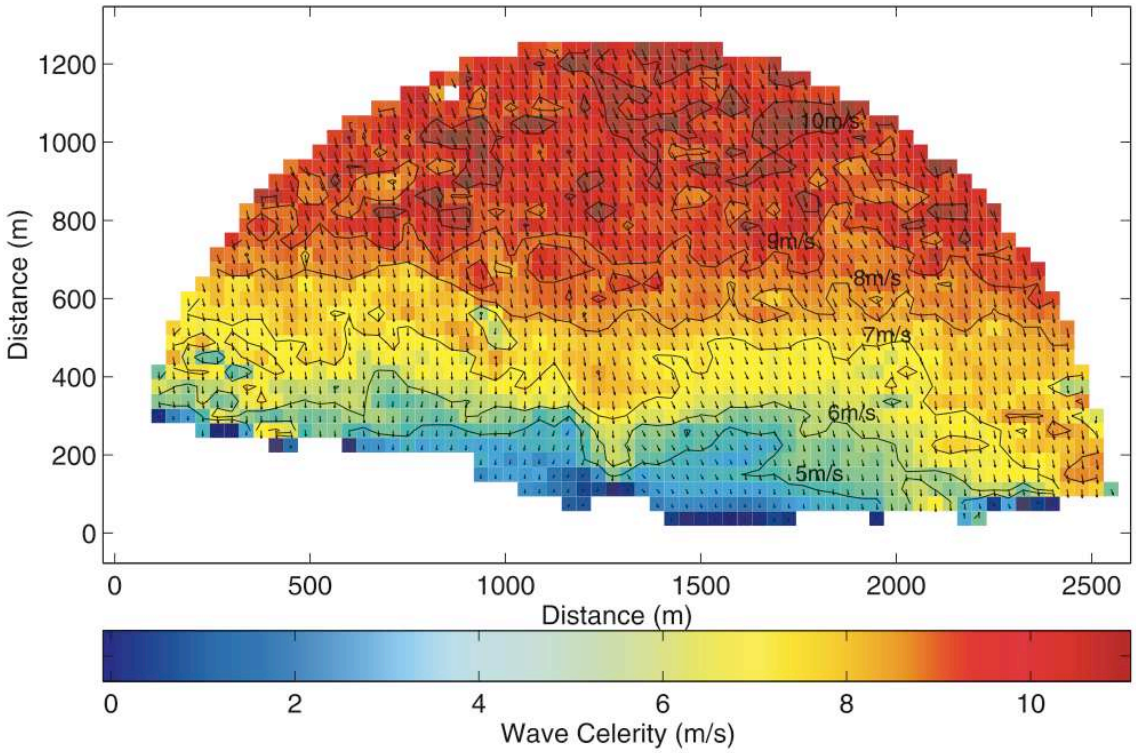

Figure 4. Plot of wave celerity from X-Band marine radar (From Bell, 1999)

Figure 5 is a plot of water depth as calculated from the wave celerity data in Figure 4 by the linear dispersion relationship calculation (Bell, 1999).

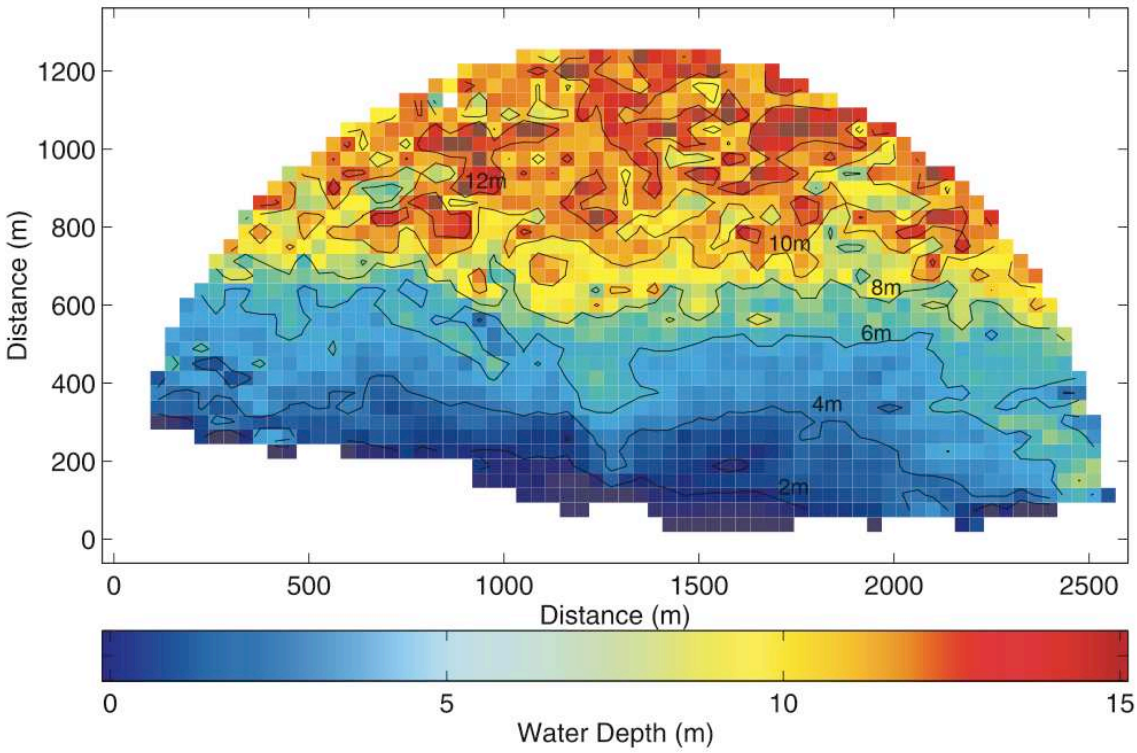

Figure 5. Plot of water depth calculated from X-Band radar data (From Bell, 1999)

A long dwell time, of approximately 100 seconds is required for the three dimensional Fourier Transform analyses, which is not practical for remote sensing type platforms. Therefore, a study was conducted from data collected with the Imaging Science Research radar located on the pier of the U.S. Army Corps of Engineers Field Research Facility, Duck, NC to test the potential for determining bathymetry for small X-Band radars mounted on aircraft or Unmanned Aerial Vehicles (UAV) with much smaller dwell times of approximately 10 seconds (Abileah & Trizna, 2010). The 10-second dwell time for aircraft is much less than the 100-second dwell time required for the three-dimensional Fourier analyses, so for this study a two-dimensional Fourier Transform analyses of the data were used. The two-dimensional Fourier analyses actually results in a number of advantages over the three-dimensional analyses. Fewer images are required; in fact depth can be estimated with as few as two images. Also, depth accuracy no longer depends on time; it only depends on the signal to noise ratio (SNR). In fact, if the SNR is high enough depth can be accurately determined with as few as two images and a dwell

time as short as ten seconds. Figure 6 is a plot of water depth calculated from X-Band radar data estimated with two-dimensional Fourier analyses and overlaid on an aerial image of Duck, NC (Abileah & Trizna, 2010).

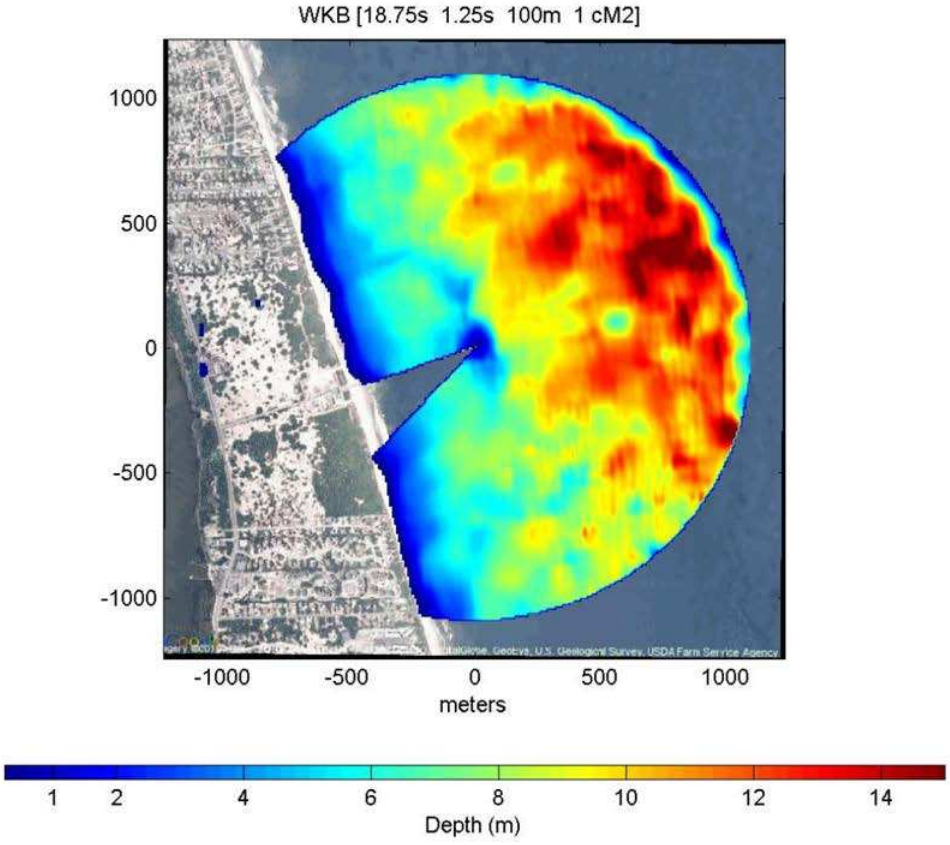

Figure 6. Plot of water depth calculated from X-Band radar data using 2D analyses (From Abileah & Trizna, 2010)

b. Video Imagery and Wave number

Video imagery can also determine nearshore bathymetry by applying the linear dispersion relationship for surface gravity waves. The video technique first estimates the frequency of the wave, which involves the collection of pixel intensity time series at an array of pixel locations. Average spectrum is then calculated and the spectral peak is selected as the frequency corresponding to the wave celerity. The cross-shore wave number is then estimated by analysis of wave phase structure through a frequency domain complex empirical orthogonal function (CEOF). The wave number is then used

to calculate depth by the linear dispersion relationship of surface gravity waves. Figure 7 is a plot of estimated wave angle and water depths for Duck, NC calculated by the video technique. Figure 7 (b) compares the estimated water depths to the ground truth as collected by Coastal Research Amphibious Buggy (CRAB) for the same day (Stockdon & Holman, 2000).

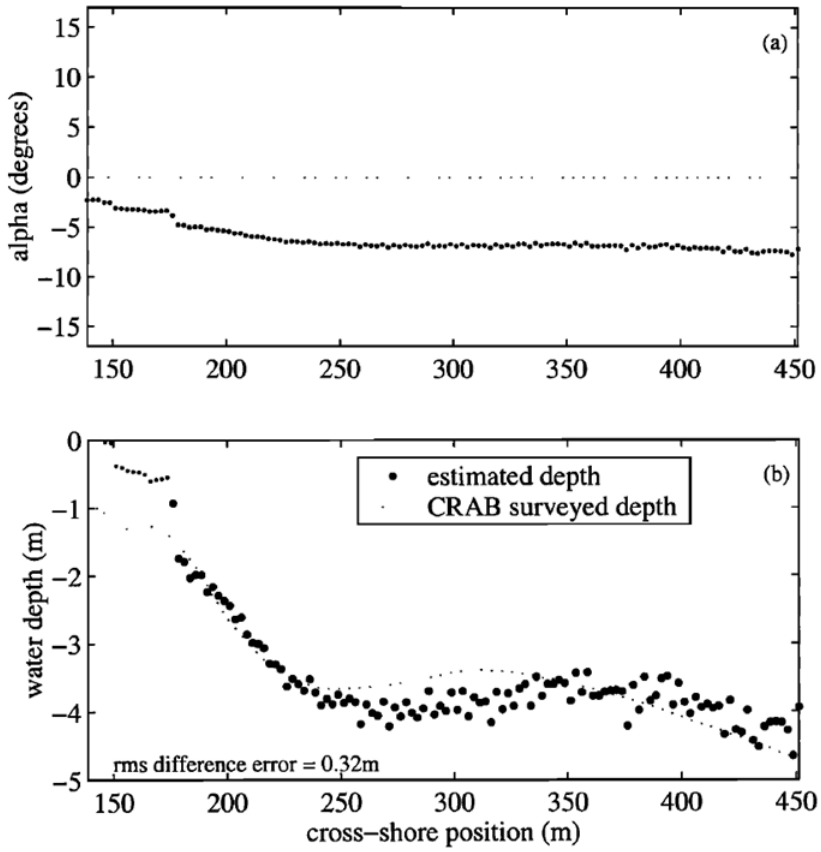

Figure 7. Plot of wave angle and water depth estimates for Duck, NC using video technique (From Stockdon & Holman, 2000)

Decoupling the wave number estimation from the water depth estimation provides improved spatial resolution and quantitative error predictions, and is well suited to solve the bathymetry inversion problem (Plant, Holland, & Haller, 2008). This is accomplished by deriving a formal inverse model that solves for the unknown spatially variable wave numbers from image sequences vice solving for wave celerity independently (Plant et al., 2008). One advantage of separating the depth estimation

from the wave number estimation is that it results in quantitatively accurate bathymetric error predictions since each depth estimation is based on independent wave number estimations (Plant et al., 2008).

c. Satellite Imagery

In 2005, nearshore bathymetry was determined from satellite imagery by applying the linear dispersion relationship of surface gravity waves to a series of seven pan-multispectral image sets of the inlet into San Diego harbor from the IKONOS satellite. Two-dimensional Fourier Transforms are conducted on the images to convert image intensity into wave numbers. Then, the phase change of two or more images is transformed to derive both depth and current from the linear dispersion relationship. In Figure 8, the image on the left depicts the bathymetry of San Diego Harbor by this method and the image on the right is the ground truth bathymetry of San Diego Harbor as determined six months after the satellite imagery from a Fugro West multibeam SONAR survey. This comparison demonstrates that nearshore bathymetry is accurately determined from satellite imagery by the linear dispersion relationship of surface gravity waves with one-sigma depth errors of only four to seven percent (Abileah, 2006).

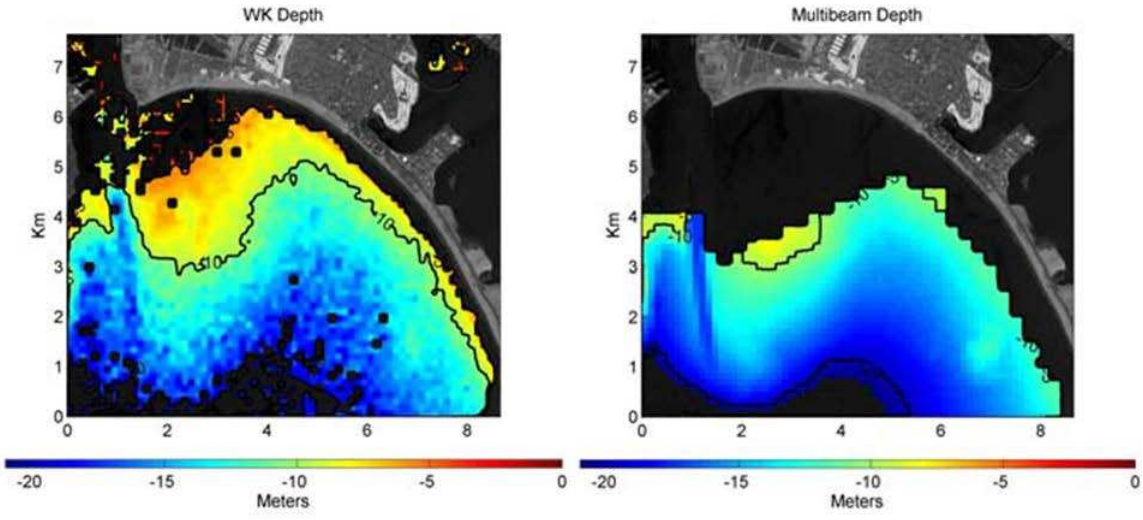

Figure 8. Bathymetry of San Diego Harbor estimated by IKONOS (left) compared with Fugro multibeam depth (right) (From Abileah, 2006)

d. Neuro-Fuzzy Technique

The Neuro-fuzzy technique is an optical depth technique that depends on an Adaptive-Network-based Fuzzy Inference System (ANFIS) to determine nearshore bathymetry from multispectral satellite images. An adaptive network is a feed-forward neural network where each node performs a specific function and no weights associated to the links between different nodes (Corucci, Masini, & Cococcioni, 2011). This avoids systematic uncertainties because the algorithm is trained only on real data. Adaptive networks rely on a collection of input-output data pairs in order to determine the model structure. In this case the three Quickbird visible bands are the input and estimated depth is the system output. Accurate bathymetry of the area off the coast of Grosseto, Italy was determined by this method from two multispectral Quickbird images. The accuracy obtained by this method was comparable to the accuracy achieved by the linear dispersion relationship applied to the IKONOS images. However, the ANFIS method requires a significant amount of predetermined depths to represent the desired output from the system. These predetermined depths are then divided into three datasets: a test set, ANFIS validation set, and ANFIS training set (Corucci et al., 2011). This is not practical when dealing with denied or hostile areas, thus making this method impractical for an operational capability to determine bathymetry of denied or hostile areas in support of amphibious operations or mine warfare planning. Figure 9 is a plot of the estimated depth as determined by ANFIS from the 2008 Quickbird image of Grosseto, Italy, versus the predetermined depths. The 2008 image is the more realistic of the two images as there were limited number of predetermined depths associated with that image (Corucci et al., 2011).

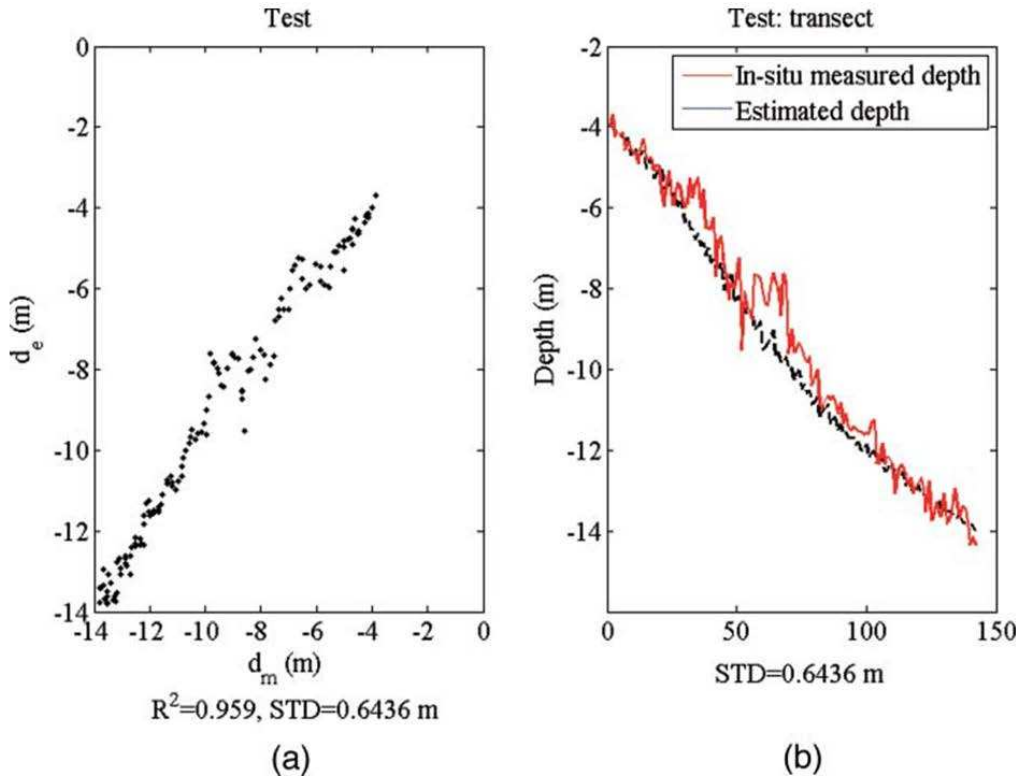

Figure 9. Plot of estimated depth by ANFIS versus predetermined depth (From Corucci et al., 2011)

B. THEORY

1. Periodic Waves

All periodic waves are characterized by the same key parameters: wave length (L), the horizontal distance from crest to crest; wave height (H), the vertical distance from trough to crest; and period (T), the time interval between the appearances of successive crests at the same point. Figure 10 is a graphical depiction of these key parameters. The frequency (f) of a wave is defined as the number of waves per unit time and is expressed as (Komar, 1998; Caruthers et al., 1985):

$$f = 1/T \tag{1}$$

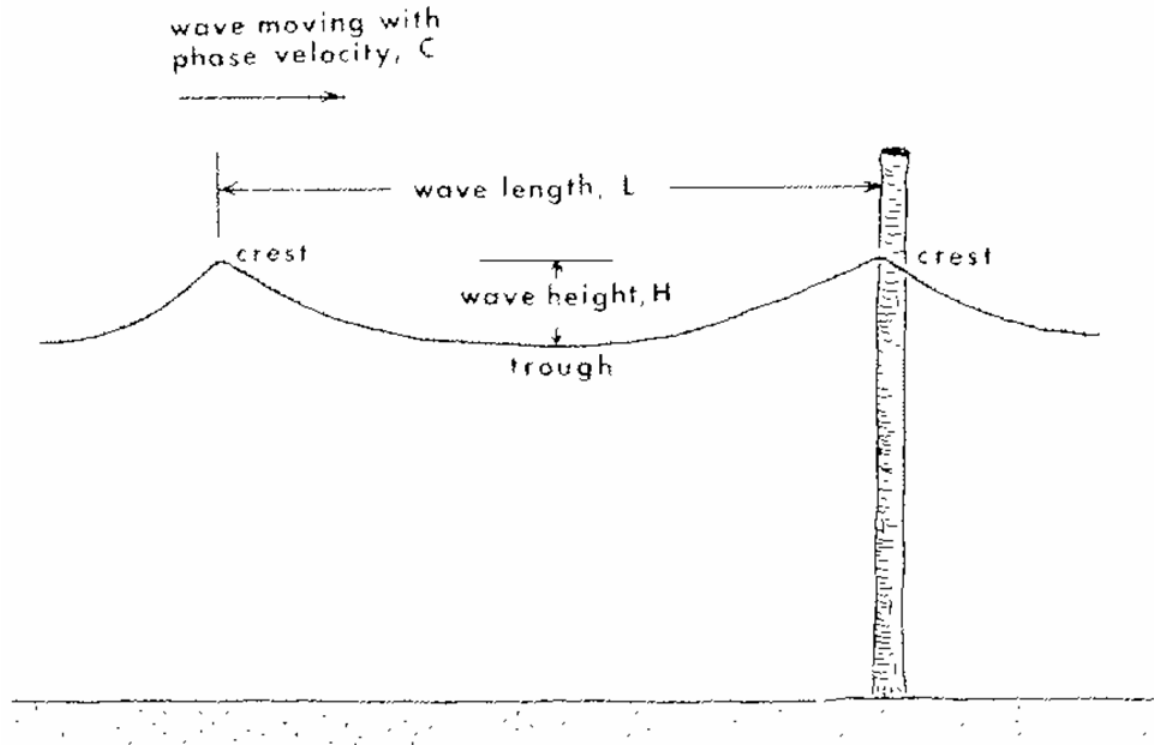

Figure 10. General Wave Characteristics (From Komar, 1998)

The wave frequency is the number of waves per unit time and period is time for one full wave length to pass a given point, then the celerity of the wave can be expressed as (Komar, 1998):

$$C = L / T \tag{2}$$

where C is defined as the wave phase velocity or wave celerity. Longer Period waves travel faster. This leads to the waves sorting themselves out based on their periods as they advance from the generation point to the shore, which is referred to as wave dispersion and results in a smooth regular undulation of the ocean water with a narrow range of periods called swell (Komar, 1998).

2. Linear Airy-Wave

Linear Airy-wave theory is the simplest of the wave theories. For this theory it is assumed that wave height is much smaller than both the wave length and depth. A fundamental relationship derived from Linear Airy-wave theory is the dispersion equation (Komar, 1998):

$$\sigma^2 = gk \tanh(kh) \tag{3}$$

where $\sigma = 2\pi / T$ is the angular frequency, g is the acceleration due to gravity, $k = 2\pi / L$ is the wave number, and h is the water depth. Substituting in the expressions for σ and k yields (Komar, 1998):

$$L = \frac{g}{2\pi} T^2 \tanh\left(\frac{2\pi h}{L}\right) \tag{4}$$

In deep water, where the wave length is small as compared to the depth ($h > L_0 / 2$), the expression $\left(\frac{2\pi h}{L}\right)$ becomes large thus $\tanh\left(\frac{2\pi h}{L}\right) \approx 1$ and Equation (4) can be reduced to (Komar, 1998):

$$L_0 = \frac{g}{2\pi} T^2 \tag{5}$$

Now substituting Equation (5) into Equation (1), we can now write an expression for the deep water wave celerity:

$$C_0 = \frac{g}{2\pi} T \tag{6}$$

For deep water waves, wave celerity and wave length are constant and only depend on the period, wave height is also constant. Deep water waves do not feel the bottom and therefore are unaffected by the depth as shown in Figure 11 (Komar, 1998).

As the waves continue to propagate toward shore, they will begin to feel the bottom at a depth equal to approximately one half their wave length. At this point, the deep water expression can no longer be applied (Komar, 1998).

Once the waves reach shallow water where $h < L_0 / 20$, $\tanh\left(\frac{2\pi h}{L}\right)$ approaches $\left(\frac{2\pi h}{L}\right)$ and Equation 4 can be reduced to the shallow expressions (Komar, 1998):

$$L_s = T\sqrt{gh} \tag{7}$$

$$C_s = \sqrt{gh} \tag{8}$$

For shallow water waves, wave celerity and wave length depend only on depth and period remains constant. Thus, as waves enter shallow water, wave celerity decreases, wave length decreases, wave height increases and period does not change as shown in Figure 11 (Komar, 1998).

In the intermediate depth range, where $L_0 / 4 > h > L_0 / 20$, Equation 4 must be used. For waves in the intermediate depth range, wave celerity and wave length decrease as depth tends to decrease, while wave height increase as shown in Figure 11 (Komar, 1998).

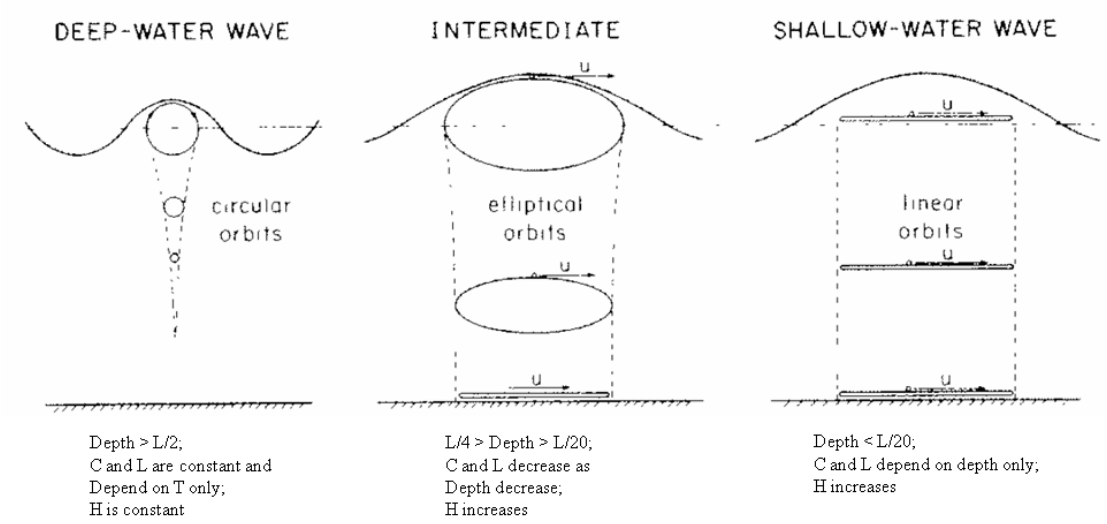

Figure 11. Linear Airy-wave approximations for varying depths (After Komar, 1998)

Table 1 summarizes the principal equations of interest derived from Linear Airy-wave theory.

Table 1. Equations derived from Linear Airy-wave theory (After Komar, 1998)

Parameter	General Expression	Deep Water	Shallow Water
Surface elevation	$\eta(x,t) = \frac{H}{2}\cos(kx - \sigma t)$		
Phase celerity	$C = \frac{gT}{2\pi}\tanh\left(\frac{2\pi h}{L}\right)$	$C_0 = \frac{gT}{2\pi}$	$C_s = \sqrt{gh}$
Wave length	$L = \frac{gT^2}{2\pi}\tanh\left(\frac{2\pi h}{L}\right)$	$L_0 = \frac{gT^2}{2\pi}$	$L_s = T\sqrt{gh}$
Horizontal orbital diameter	$d = H\frac{\cosh[k(z_0 + h)]}{\sinh(kh)}$	$d = He^{kz_0}$	$d = \frac{HL_s}{2\pi h} = \frac{HT}{2\pi}\sqrt{\frac{g}{h}}$
Vertical orbital diameter	$s = H\frac{\sinh[k(z_0 + h)]}{\sinh(kh)}$	$s = He^{kz_0}$	$s = 0$
Horizontal orbital velocity	$u = \frac{\pi H}{T}\frac{\cosh[k(z_0 + h)]}{\sinh(kh)}\cos(kx - \sigma t)$	$u = \frac{\pi H}{T}e^{kz}\cos(kx - \sigma t)$	$u = \frac{H}{2}\sqrt{\frac{g}{h}}\cos(kx - \sigma t)$
Vertical orbital velocity	$w = \frac{\pi H}{T}\frac{\sinh[k(z_0 + h)]}{\sinh(kh)}\sin(kx - \sigma t)$	$w = \frac{\pi H}{T}e^{kz}\sin(kx - \sigma t)$	$w = 0$

3. Cnoidal and Solitary Wave

Linear Airy-wave theory begins to break down when waves enter into very shallow water as the ratio H/h approaches unity, and the assumption that H is much smaller than both L and h is no longer valid (Komar, 1998). This is particularly true in the surf zone where wave height increases wave celerity (Holland, 2001). The nonlinear wave processes observed in the surf zone will result in larger wave celerities than predicted by the linear dispersion relation, resulting in over estimation of depths. In order to improve the accuracy of depth estimations in the surf zone, a higher order wave theory should be applied (Bell, 1999).

Cnoidal wave theory should be utilized for waves in the surf zone. However, this theory is seldom employed due the complexity of the analyses. The expression for Cnoidal wave celerity is:

$$c = \sqrt{g\left(h + \alpha H\right)} \tag{9}$$

where α is a function of Ursell number, $U_r = H / \left(k^2 h^3\right)$ (Komar, 1998). The Ursell number is a dimensionless parameter used in fluid dynamics to indicate the nonlinearity of long surface gravity waves on a fluid layer. Solitary wave theory is a limiting case of the Cnoidal wave theory where $\alpha = 1$ (Holland, 2001). Solitary wave consist of a single crest and does not have wave period or wave length associated with it (Komar, 1998). Solitary wave theory accounts for the effects of wave height on wave celerity but removes the complicated function of Ursell number (Stockdon & Holman, 2000). Thus, the equation for wave celerity for a solitary wave is:

$$c = \sqrt{g\left(h + H\right)} \tag{10}$$

Figure 12 compares the theoretical wave forms based on Solitary, Cnoidal, and Linear Airy-wave theories.

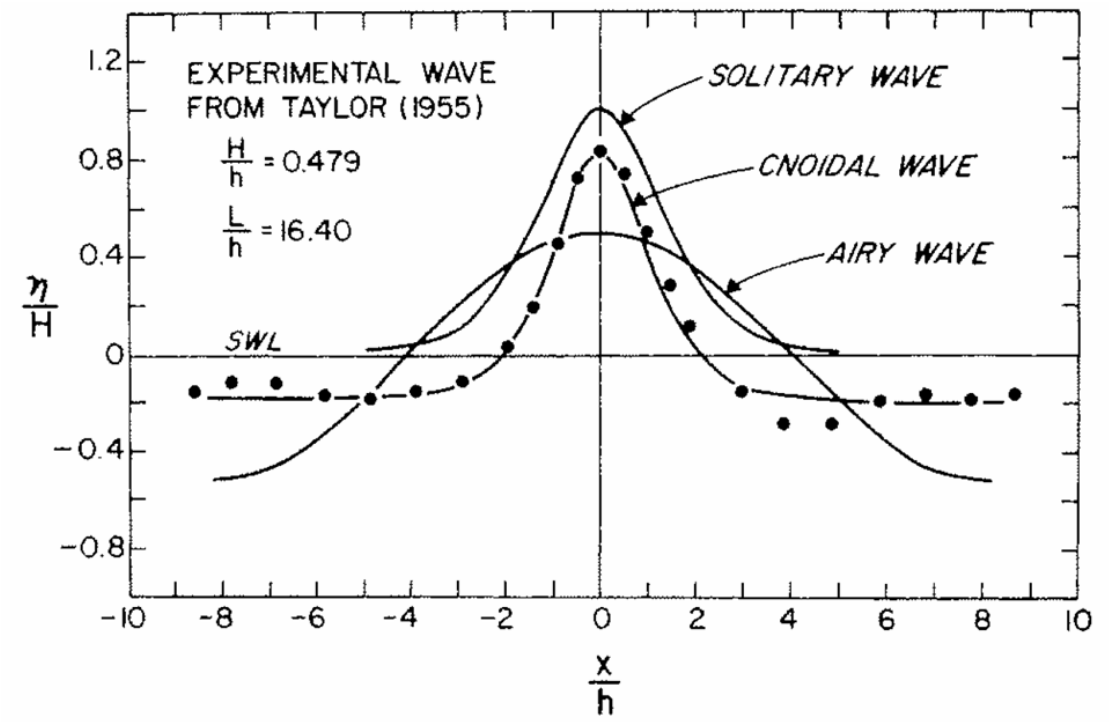

Figure 12. Comparison of Solitary, Cnoidal, and Airy wave profiles (From Komar, 1998)

III. PROBLEM

A. DEFINITION

The capability to remotely determine subaqueous beach profiles of remote, denied, or hostile areas is critical to providing proper IPE in support of amphibious operations, mine warfare, and/or HADR planning. "The Navy, in support of amphibious operations, also requires the ability to remotely and surreptitiously determine the bathymetry profile of the ocean near amphibious landing zones" (OPNAV N2/N6, 2010). Remote sensing satellites in LEO provide the best access into these areas. The problem lies in determining the best method for producing subaqueous beach profiles from remote sensing data. The wave celerity method by the linear dispersion relationship for surface gravity waves is a convenient method to accurately estimate nearshore subaqueous beach profiles, but it requires 2-meter resolution in order to resolve the waves and the ability to obtain multiple images in short succession.

This study was conducted as a proof of concept to demonstrate that commercial satellite imagery has sufficient capability to meet the above requirements, and solve the problem of determining bathymetric profiles of denied or hostile areas. This study used multispectral imagery acquired by the WorldView-2 satellite to determine the bathymetric profile of the coastal area near Camp Pendleton, California.

B. MATERIALS

1. WorldView-2 Sensor

WorldView-2 satellite collected ten images in rapid succession of the coastal area off Camp Pendleton. WorldView-2 is a high resolution 8-band multispectral commercial imaging satellite owned and operated by DigitalGlobe (Figure 13). It was launched in October 2009. WorldView-2 is capable of 46 cm panchromatic resolution at nadir and 1.85 m multispectral resolution at nadir (DigitalGlobe, 2011).

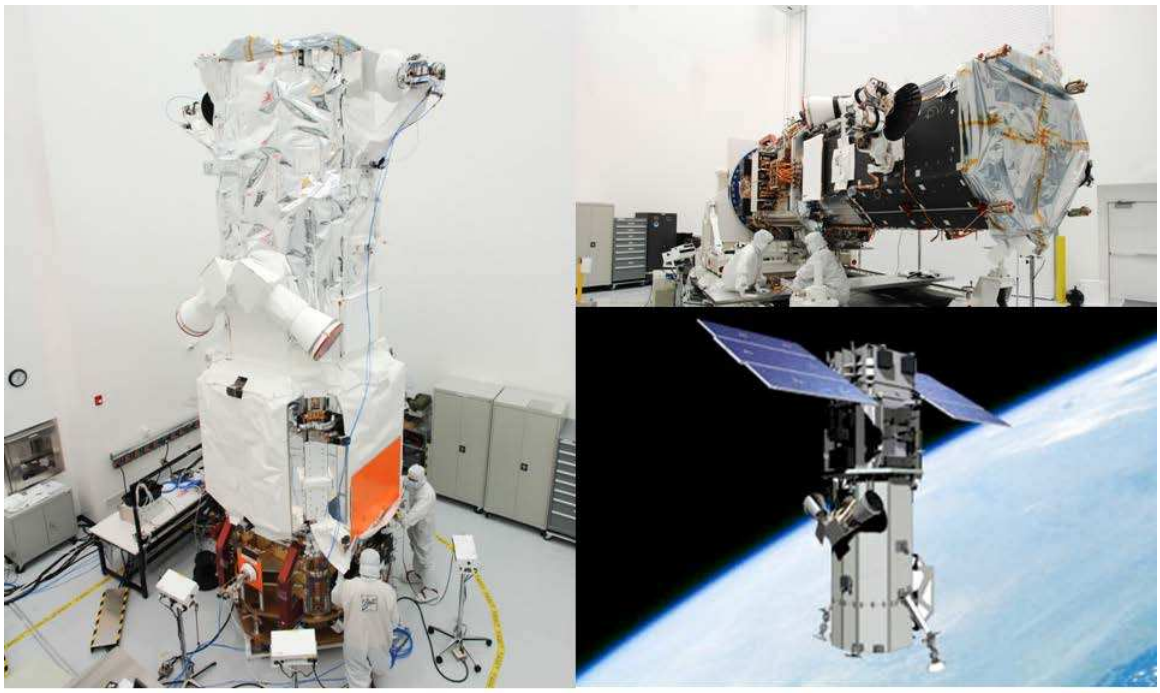

Figure 13. WorldView-2 Satellite (From DigitalGlobe)

WorldView-2 is the first satellite to combine high resolution panchromatic with 8-band multispectral sensor capabilities giving it significant spectral performance improvement over the other two satellites in DigitalGlobe's fleet, QuickBird and WorldView-1. In addition to the four standard color bands of blue, green, red, and near infrared, WorldView-2 adds four new color bands: coastal blue, yellow, red edge, and a second band of near infrared. Figure 14 shows wave lengths covered by each band as well as, the increased spectral coverage as compared to the other two DigitalGlobe satellites (DigitalGlobe, 2010; DigitalGlobe, 2010; DigitalGlobe, 2011).

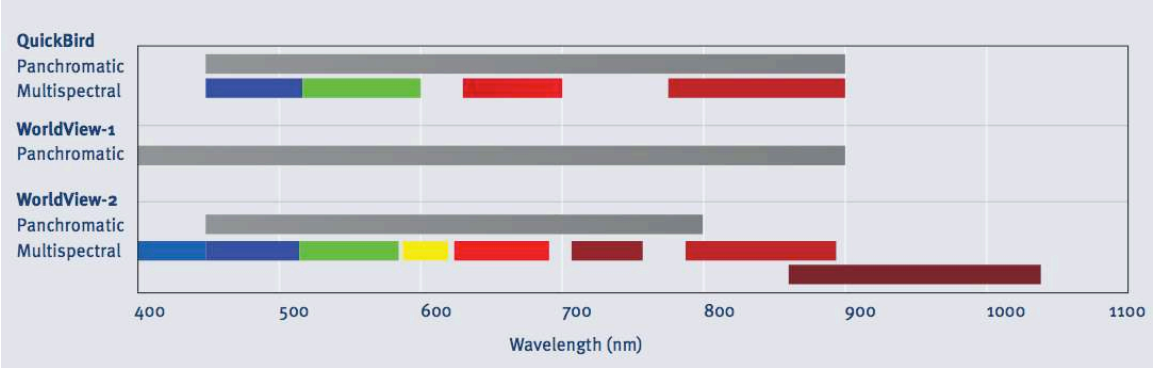

Figure 14. DigitalGlobe satellite spectral coverage (From DigitalGlobe, 2010)

The WorldView-2 satellite can achieve an acceleration of 1.43 deg/s/s and a rate of 3.86 deg/s allowing it to slew 200 km in 10 seconds. This increased retargeting agility allows for multiple images of the same area to be taken in rapid succession. Table 2 lists key parameters and specifications for the WorldView-2 satellite.

Table 2. WorldView-2 Specifications (After DigitalGlobe, 2011)

Launch Information	Date: October 8, 2009 Launch Vehicle: Delta 7920 (9 strap-ons) Launch Site: Vandenberg Air Force Base, California
Orbit	Altitude: 770 kilometers Type: Sun synchronous, 10:30 am descending node Period: 100 minutes
Mission Life	7.25 years, including all consumables and degradables (e.g. propellant)
Spacecraft Size, Mass and Power	4.3 meters (14 feet) tall x 2.5 meters (8 feet) across 7.1 meters (23 feet) across the deployed solar arrays 2800 kilograms (6200 pounds) 3.2 kW solar array, 100 Ahr battery
Sensor Bands	Panchromatic: 450 - 800 nm 8 Multispectral: Coastal: 400 - 450 nm Red: 630 - 690 nm Blue: 450 - 510 nm Red Edge: 705 - 745 nm Green: 510 - 580 nm Near-IR1: 770 - 895 nm Yellow: 585 - 625 nm Near-IR2: 860 - 1040 nm
Sensor Resolution	Panchromatic: 0.46 meters GSD at nadir*, 0.52 meters GSD at 20° off-nadir Multispectral: 1.84 meters GSD at nadir*, 2.08 meters GSD at 20° off-nadir
Dynamic Range	11-bits per pixel
Swath Width	16.4 kilometers at nadir

2. The Environment for Visualizing Images 4.7 (ENVI)

The Environment for Visualizing Images software version 4.7 was used in this study to process the WorldView-2 imagery in order to resolve the wave crest. ENVI 4.7 is a software application produced by ITT Visual Information Solutions for processing and analyzing geospatial imagery. ENVI 4.7 contains a number of features, functionality and tools for extracting information from geospatial imagery (*ENVI, IDL, & Industry Brochures from ITT Visual Information Solutions*). For this study, features such as; change detection, Fourier Transforms, Principal Component Transforms, image registration, filtering, and measurement tools extracted the needed information from the WorldView-2 imagery.

3. USGS Digital Elevation Model for Southern California

The USGS DEM for Southern California data series 487 provided ground truth data for this study. The estimated depths calculated for this study were compared to this USGS DEM to determine accuracy of the methods. This DEM was constructed in 2009 by integrating over forty of the most recent bathymetric and topographic data sets collected by LIDAR, multibean and single beam SONAR, and Interferometric Synthetic Aperture Radar (IfSAR). Forty-five individual DEMs were constructed from these datasets. Figure 15 shows the location of these 45 DEMs, and Table 3 is a list of the DEM identifiers and respective locations of each. For this study, DEM sd10 was used (Barnard & Hoover, 2010).

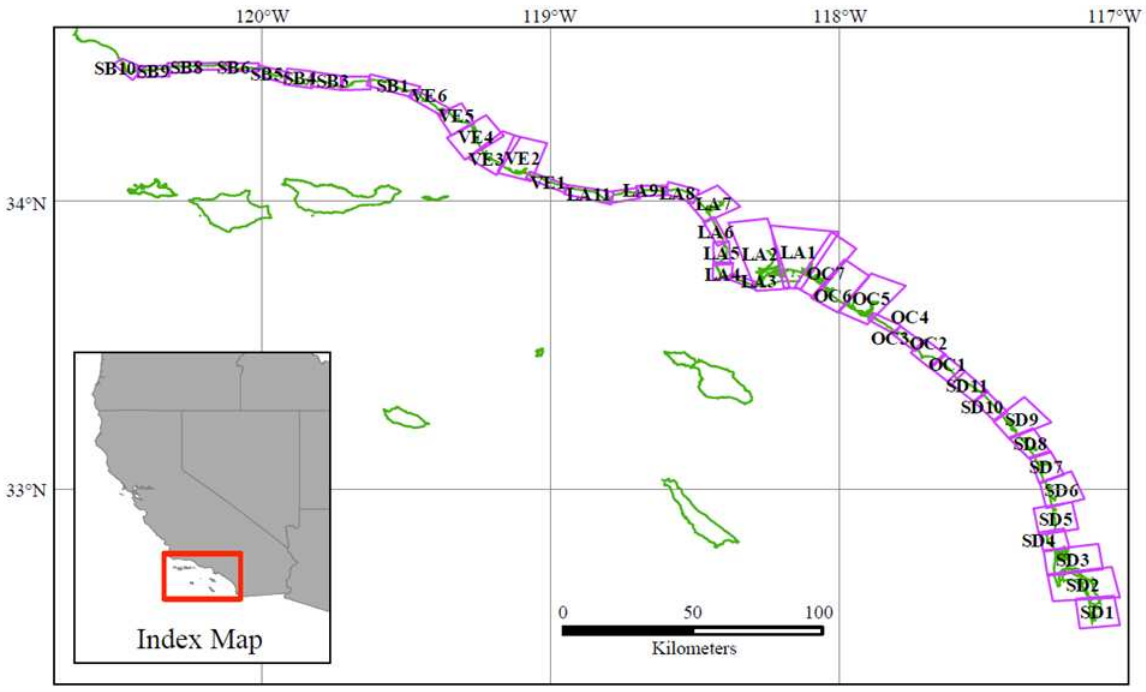

Figure 15. USGS location map and identifiers (IDs) for the 45 DEMs (From Barnard & Hoover, 2010)

Table 3. USGS Individual DEM names and locations (From Barnard & Hoover, 2010)

DEM ID	Geographic Name	County
sd1	Imperial Beach	San Diego
sd2	San Diego Harbor	San Diego
sd3	Mission Bay	San Diego
sd4	La Jolla	San Diego
sd5	Torrey Pines	San Diego
sd6	Del Mar/Solana/Cardiff	San Diego
sd7	Encinitas	San Diego
sd8	Carlsbad	San Diego
sd9	Oceanside	San Diego
sd10	Camp Pendleton	San Diego
sd11	San Onofre	San Diego
oc1	San Clemente	Orange
oc2	Dana Point	Orange
oc3	Laguna Beach South	Orange
oc4	Laguna Beach North	Orange
oc5	Newport Beach	Orange
oc6	Huntington Beach	Orange
oc7	Seal Beach	Orange
la1	Port of Long Beach	Los Angeles
la2	Port of Los Angeles	Los Angeles
la3	San Pedro	Los Angeles
la4	Palos Verdes	Los Angeles
la5	Redondo Beach	Los Angeles

DEM ID	Geographic Name	County
la6	Manhattan Beach	Los Angeles
la7	Marina Del Rey	Los Angeles
la8	Pacific Palisades	Los Angeles
la9	Malibu	Los Angeles
la10	Dume East	Los Angeles
la11	Dume West	Los Angeles
ve1	Mugu East	Ventura
ve2	Mugu West	Ventura
ve3	Channel Islands Harbor	Ventura
ve4	Santa Clara River	Ventura
ve5	Ventura	Ventura
ve6	Rincon	Ventura
sb1	Carpinteria	Santa Barbara
sb2	Santa Barbara East (Harbor)	Santa Barbara
sb3	Santa Barbara West	Santa Barbara
sb4	UC Santa Barbara	Santa Barbara
sb5	Dos Pueblos	Santa Barbara
sb6	Tajiguas	Santa Barbara
sb7	Gaviota East	Santa Barbara
sb8	Gaviota West	Santa Barbara
sb9	Sacate	Santa Barbara
sb10	Point Conception	Santa Barbara

THIS PAGE INTENTIONALLY LEFT BLANK

IV. METHODS AND OBSERVATIONS

A. WORLDVIEW-2 IMAGERY OF CAMP PENDLETON

1. Collection

The imagery of the littoral region near Camp Pendleton, CA was collected on March 24, 2010, by DigitalGlobe's WorldView-2 satellite. Ten panchromatic and multispectral images were collected in rapid succession during a single pass. Figure 16 shows a movie of the collection simulation created by Satellite Tool Kit (STK) from Analytical Graphics, Inc. (AGI).

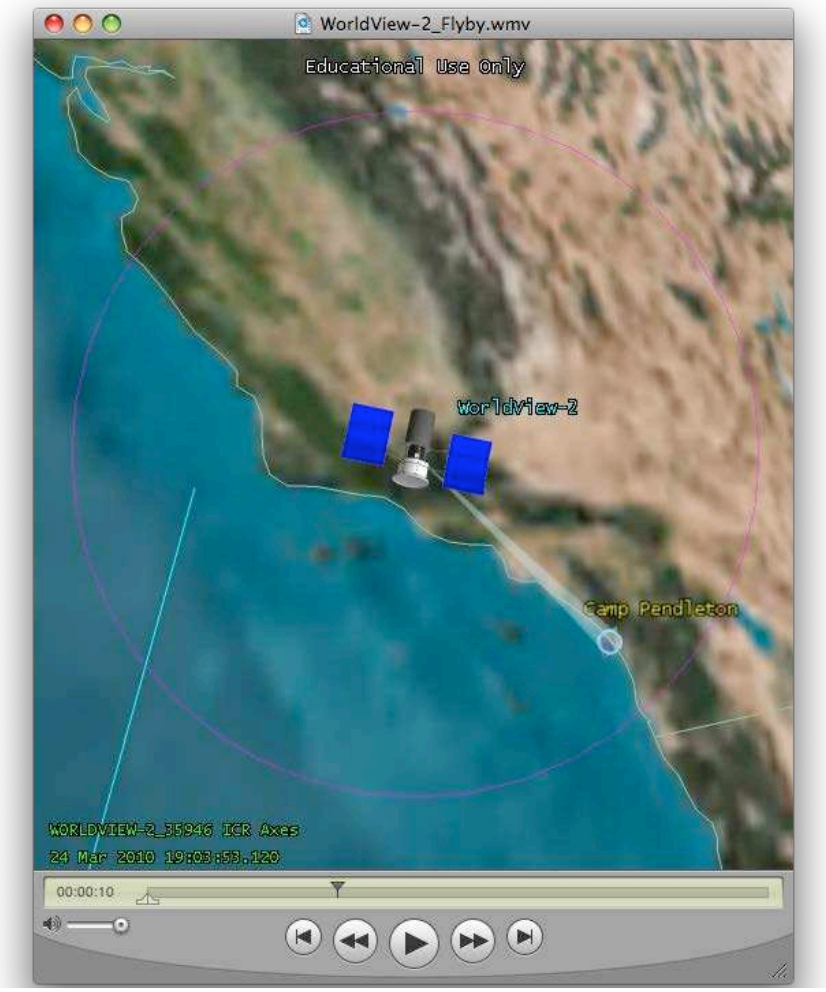

Figure 16. STK simulation of WorldView-2 Camp Pendleton area collection (From McCarthy & Naval Postgraduate School [U.S.], 2010)

DigitalGlobe provided the images in ortho-ready standard 2A format and geographic latitude/longitude coordinates. Each of the ten imagery products were delivered as three scenes approximately full swath width of 16.4 km and cut into 14 km lengths with at least 1.8 km overlap between each scene (DigitalGlobe). The total imagery product for each of the ten images consisted of three scenes identified as R1C1, R2C1, and R3C1. Figure 17 shows the basic imagery products that are divided up and delivered as scenes by DigitialGlobe. Figure 18 is a Google Earth representation of the layout of scenes R1C1, R2C1, and R3C1 from the basic imagery product of the first image of the Camp Pendleton imagery. The blue shaded area represents scene R1C1, the green shaded area represents scene R2C1, and the red shaded area represents the scene R3C1.

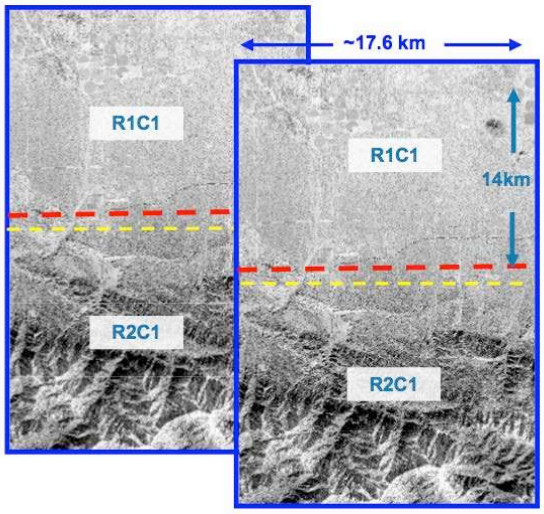

Figure 17. Physical Structure of Imagery Scenes (From DigitalGlobe)

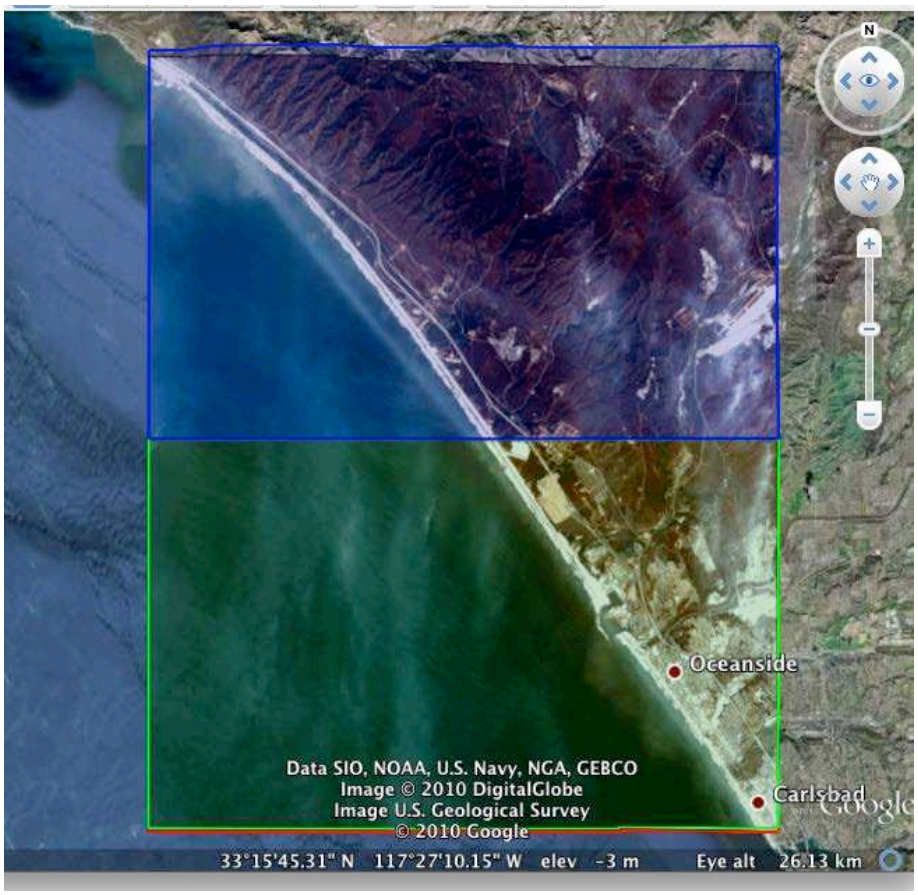

Figure 18. Google Earth representation of WorldView-2 data for Camp Pendleton area (From McCarthy & Naval Postgraduate School (U.S.), 2010)

Table 4 is a summary of the information derived from the image meta-data for each of the ten images collected. The last column in Table 4 shows the time interval between each of the successive images in this data set.

Table 4. Summary of image meta-data information (From McCarthy & Naval Postgraduate School, 2010)

WorldView-2 Data: March 24, 2010						
Directory Name: 052365928020_01						
Folder Name	**Mean GSD X**	**Mean GSD Y**	**Mean Sat AZ**	**Mean Sat EL**	**First Line Time**	**Delta Time**
P002_MUL	2.087	2.374	277.8	61.2	19:03:31.83	0
P007_MUL	2.102	2.425	267.1	60.1	19:03:42.63	10.80
P009_MUL	2.149	2.503	257.6	58.2	19:03:53.43	10.80
P006_MUL	2.229	2.609	249.5	55.8	19:04:04.23	10.80
P008_MUL	2.337	2.741	242.9	53.1	19:04:14.83	10.60
P004_MUL	2.481	2.910	237.3	50.1	19:04:25.83	11.00
P010_MUL	2.647	3.107	232.9	47.2	19:04:36.43	10.60
P005_MUL	2.841	3.338	229.2	44.4	19:04:47.03	10.60
P003_MUL	3.057	3.603	226.2	41.6	19:04:57.43	10.40
P001_MUL	3.299	3.908	223.6	39.1	19:05:07.83	10.40

2. Image Processing

a. Image Registration

The imagery was provided in ortho-ready standard 2A format as previously mentioned. In this format, the image is projected onto a reference ellipsoid using a constant base elevation with no topographic relief applied. This makes the imagery suitable for orthorectification (DigitalGlobe). Images P002, P007 and P009 were registered to the middle image P008 (Table 4) in ENVI by the resampling, scaling, and translation (RST) method with nearest neighbor resampling. Four ground reference points were selected near the waterline for the registration of the images. The first ground reference point was located in the upper left corner of the image, the second near the bottom of the image, the third and fourth near the center of the coastline. Figure 19 shows the locations of the ground reference points on an example image.

Figure 19. Ground reference point location for image to image registration (From McCarthy & Naval Postgraduate School [U.S.], 2010)

b. Image Rotation and Resizing

Next, the three registered images were rotated 131 degrees in an effort to align the coastline with the horizontal axis in order to allow the vertical profile function to measure wave lengths and wave distances. Figure 20 shows the results of this rotation.

Figure 20. Image rotation 131 degrees

After the images were rotated, they were then resized with ENVI to focus on the coast line and shallow water area for bathymetry determination. All three images were resized using a spatial subset of the image reducing the number of lines from 17404 to 2500. This was done to reduce the size of the image in order to make it more manageable for data extraction. Figure 21 shows the final size and layout of the images used for bathymetry determination following the initial image processing in ENVI.

Figure 21. Resized Image

3. Principal Component Transforms

Principal component transforms were performed on images P007 and P009 in ENVI to aid in wave detection. Principle component transform is a transformation process that rotates the data space into a coordinate system in which the different bands are uncorrelated to aid in target detection (Olsen, 2007). The eight band multispectral imagery provided by the WorldView-2 gave increased degrees of freedom for the principal component transforms to aid in target detection of wave crest. Figure 22 shows each of the eight original bands for image P007. Figure 23 shows the eight principal component bands for image P007. Principal component 4 clearly resolves the wave crest in the surf zone as distinct narrow lines.

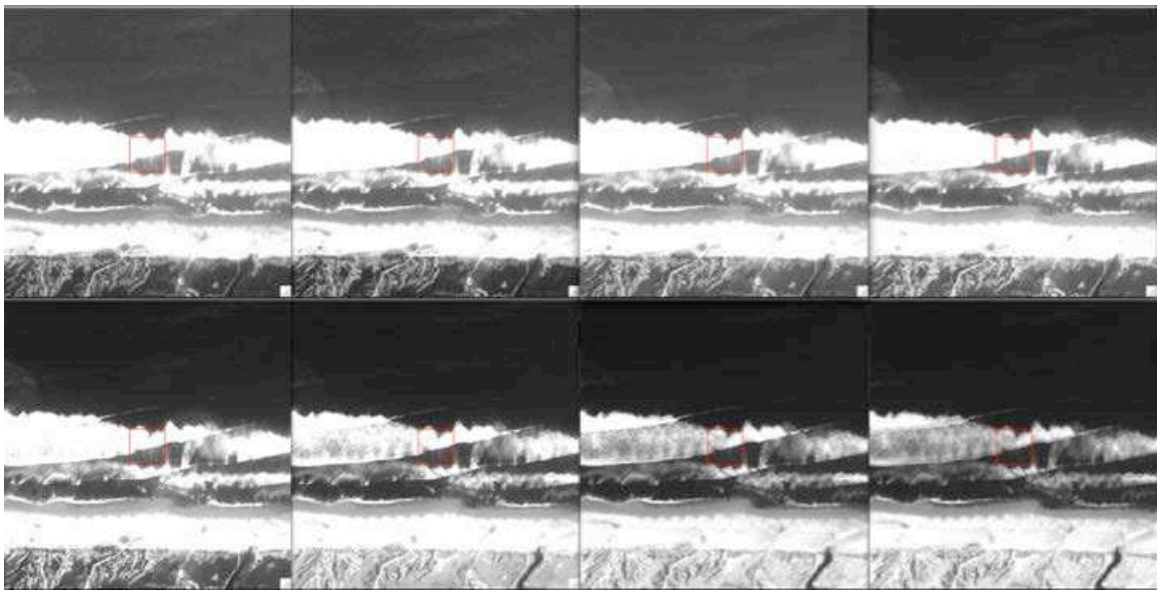

Figure 22. Original Eight Bands for image P007

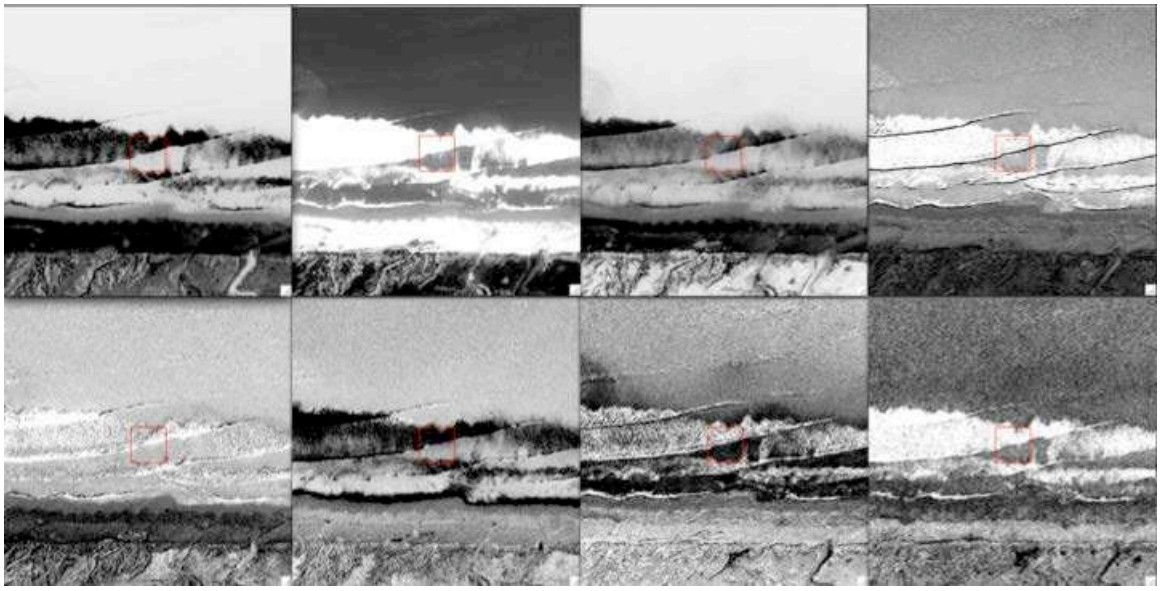

Figure 23. Eight Principal Component Banks for image P007

B. SURF ZONE

The resulting principal component four images from both images P007 and P009 where used to create a change detection image in order to determine wave celerity in the surf zone. This was accomplished by placing principal component four from image P007 into both the red and green inputs and then placing principal component four from image

P009 into the blue input. Figure 24 shows the resulting change detection image. The blue lines are the highlighted wave crest from principal component four from image P007 and the yellow lines are the highlighted wave crest from principal component four from image P009. Distance between the blue and yellow wave crest was then determined with the ENVI measurement tool. Wave celerity was then calculated using the time between images from Table 4. The linear dispersion relation for surface gravity waves was then applied to determine estimated depths. Wave height was observed to be minimal during the time frames of these particular images.

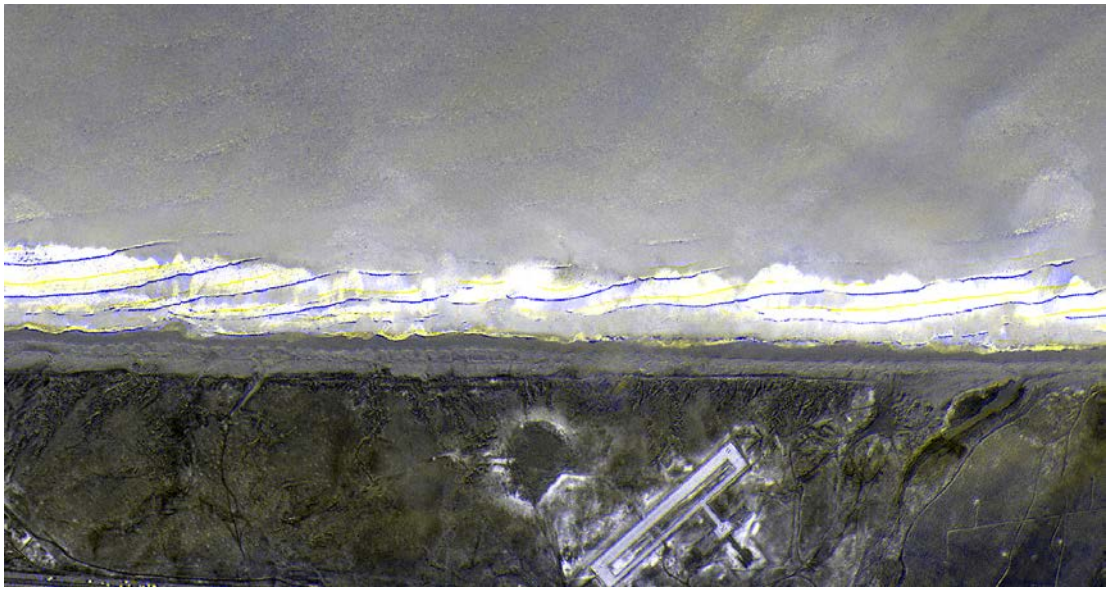

Figure 24. Change detection image for surf zone

C. OUTSIDE OF THE SURF ZONE

The principal component transform did not clearly resolve the wave crest in the shallow water as it did in the surf zone. Therefore, a change detection image was unable to be created for the area outside the surf zone and another method of determining wave celerity had to be determined. For the region outside the surf zone, the waves were first resolved by representing both images P007 and P009 in an RGB color representation of bands seven, six, and five in ENVI. These bands do not penetrate the water, resulting in increased surface wave contrast (Abileah, 2006). Then the images were enhanced by either image equalization or image linear two percent enhancement in ENVI to highlight

the wave crest. Figure 25 shows the results of this representation and enhancement of the waves.

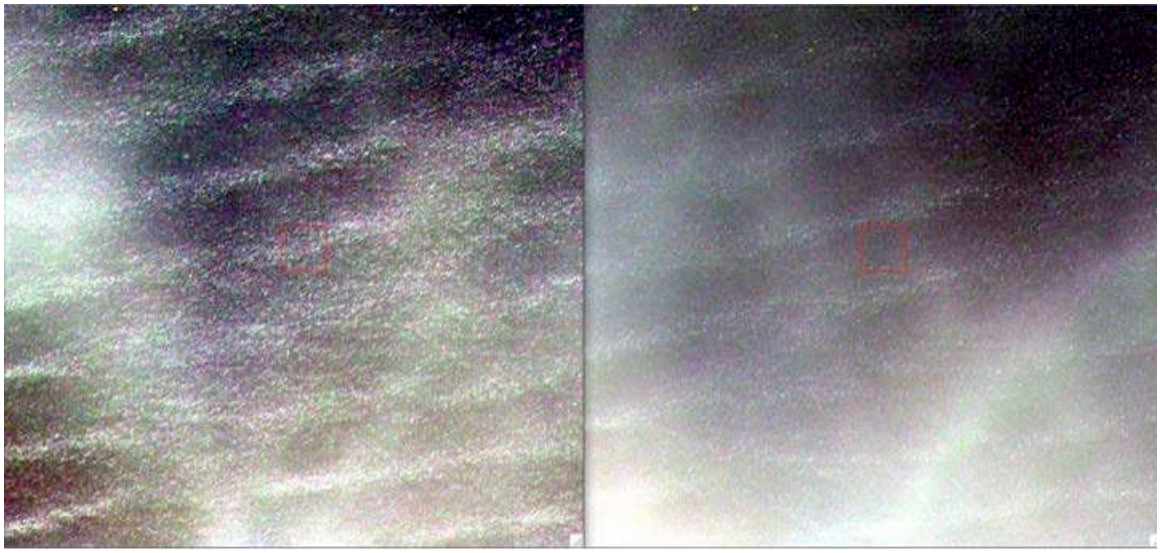

Figure 25. Image P007 (left) and P009 (right) represented by 765 bands in RGB and image equalization enhancement

The two images were linked by both linking the displays and geographic link in ENVI in order to ensure that the same area was being viewed in each image. A spatial profile was performed on each image with the vertical profile in ENVI to identify the center of the wave crest. The coordinates of the crest centers were identified with the cursor location tool in ENVI. Distance between the corresponding wave crest was then determined by the ENVI measurement tool. Wave celerity was then calculated using the time between images from Table 4. The linear dispersion relation for surface gravity waves was then applied to determine estimated depths.

THIS PAGE INTENTIONALLY LEFT BLANK

V. ANALYSIS

A. SURF ZONE

Depth was estimated in the Surf Zone by the wave celerity method. The wave celerity was determined by measuring the distance the wave traveled between image P007 and P009 and then dividing by the elapsed time between the two images as obtained from Table 4. This was accomplished by measuring the distance from the blue line to the yellow line in the change detection image with the ENVI measurement tool as shown in Figure 26.

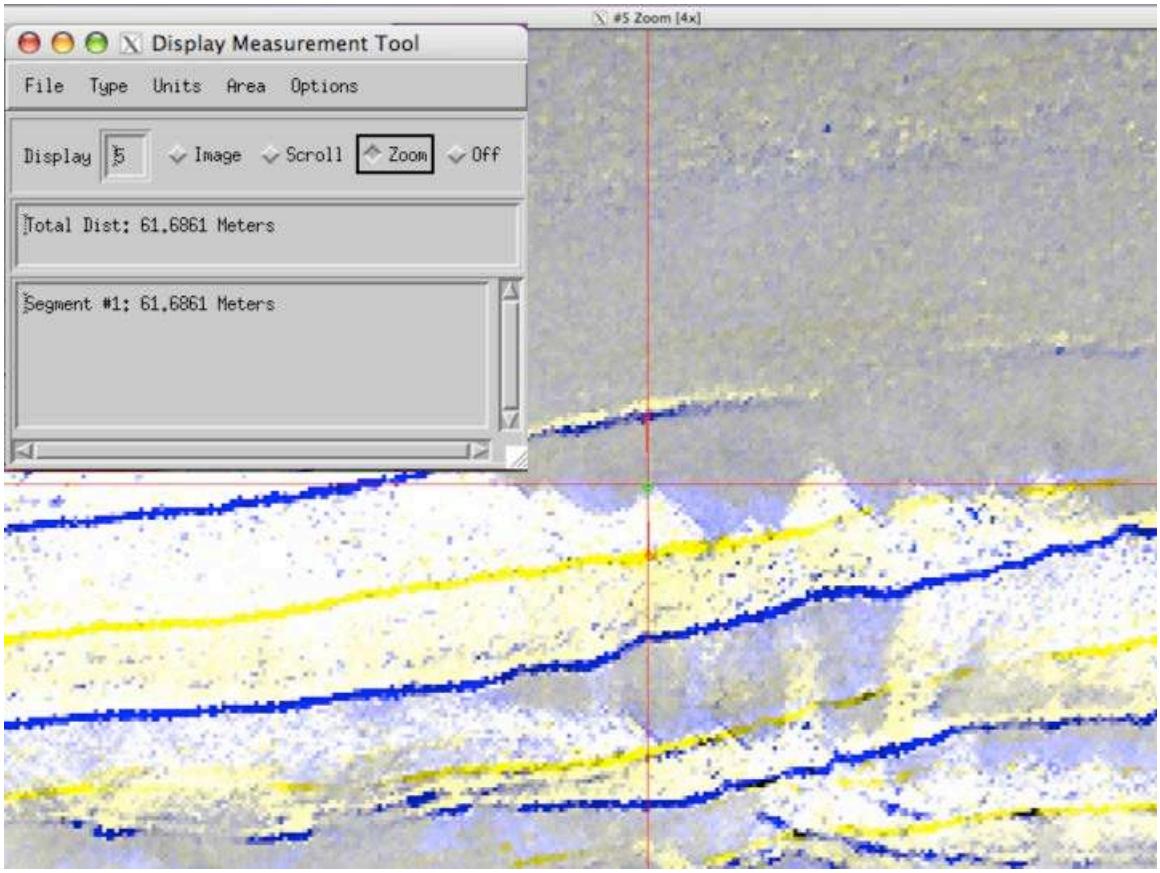

Figure 26. Calculating wave distance using ENVI measurement tool for surf zone

Once the wave celerity was calculated for each of the depth data points Equation 8 was rearranged to produce the equation:

$$h = \frac{c^2}{g} \tag{11}$$

to estimate the depth for each of the depth data points. Depth was estimated for fifty depth data points in the surf zone along the coast off Camp Pendleton. The actual points where the depth was estimated corresponds to the midpoint between the blue and yellow lines in the change detection image as indicated by the green triangle in Figure 26. The estimated depths were compared to the ground truth data. This was accomplished by first geographically linking the USGS DEM sd10 image to the change detection image in ENVI. The depth data point was located on the change detection image with the Pixel Locator tool in ENVI by the pixel coordinates associated with each depth data point. Since the two images were geographically linked the locator on the USGS image located the corresponding geographical point on the USGS image and the ground truth depth was determined from the data field of the Cursor Location/Value tool associated with the USGS image in ENVI as shown in Figure 27.

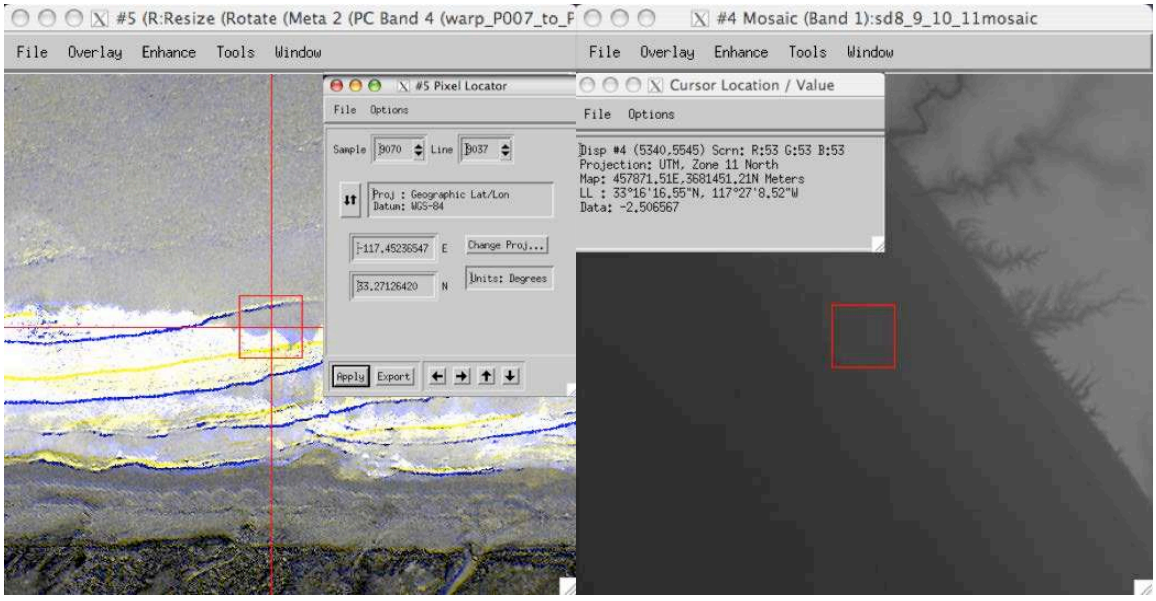

Figure 27. Ground Truth determination from USGS DEM sd10 for surf zone

The estimated depths were plotted against the ground truth depths to determine the accuracy of the wave celerity method in the surf zone (Figure 28).

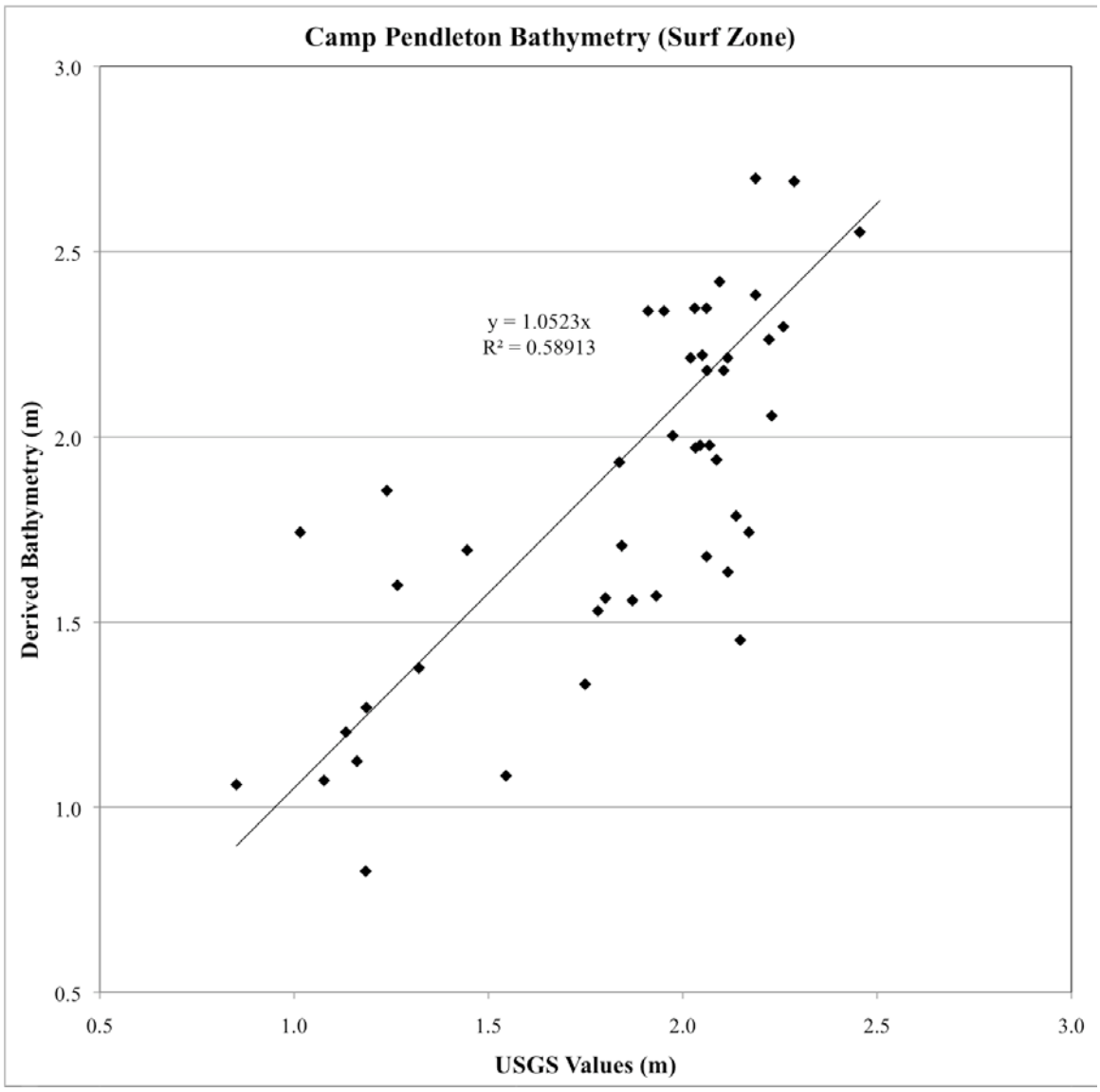

Figure 28. Plot of estimated depth versus ground truth depth in the surf zone

Figure 28 shows that on average the wave celerity method reflected a 5.2 percent error in the surf zone based on the equation for the best fit curve for the fifty depth data points with a coefficient of determination (R^2) of 0.59. The perfect model would have resulted in an equation with a slope of 1.0 and R^2 of 1.0. Sources of error include, not accounting for the wave heights in the surf zone as discussed in Chapter II, and there is a plus or minus ten percent uncertainty in the estimated depth associated with the location measurement error of plus or minus one pixel (2.4 m). The R^2 value of 0.59 says that the regression line is a good fit to the data and that it is a fair representative model. It must be noted, however, that a few individual depth estimations resulted in nearly a fifty percent over estimation of water depth. All estimated depths were within plus or minus one meter of ground truth and most were within plus or minus a half meter of ground truth. Table 6 in Appendix contains the specific results for each of the depth data points.

B. OUTSIDE OF THE SURF ZONE

Depth was estimated outside the surf zone by the wave celerity method as well; however, a change detection image for this region was not able to be produced as discussed in Chapter IV. Wave celerity was determined by measuring the distance the wave traveled between image P007 and P009 and then dividing by the elapsed time between the two images as obtained from Table 4. This was accomplished outside the surf zone by determining the pixel coordinates of the wave crest in both image P007 and P009 as discussed in Chapter IV and then using the ENVI measurement tool to measure the distance between those pixel coordinates to determine the distance the wave traveled between images as shown in Figure 29.

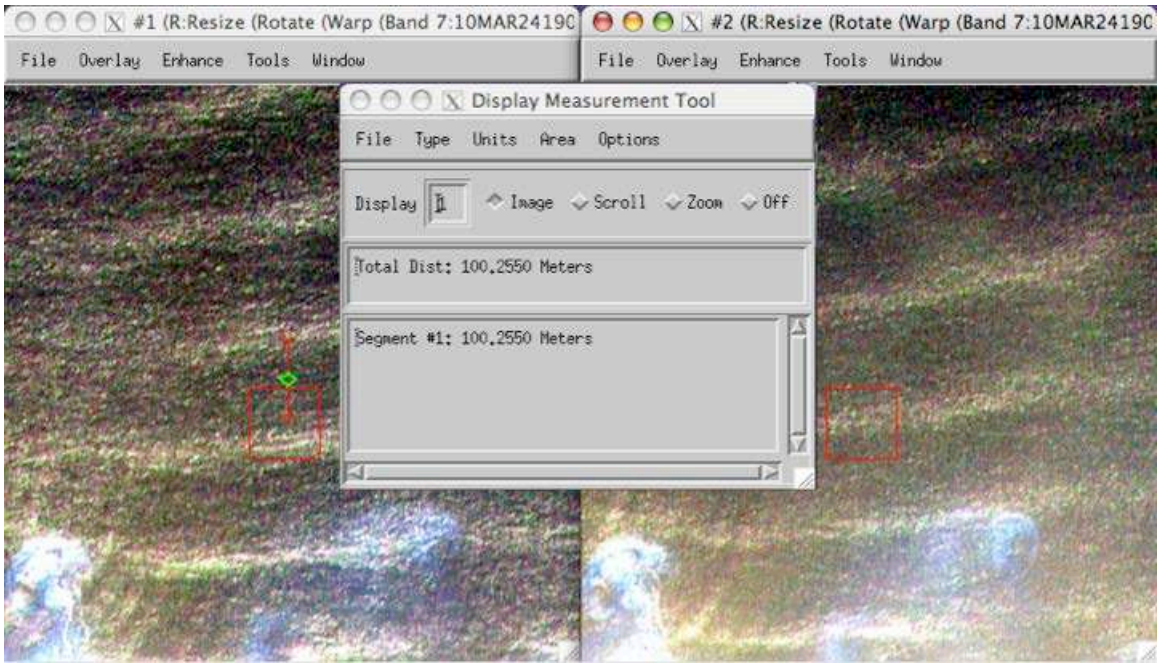

Figure 29. Calculating wave distance for outside the surf zone

Once the wave celerity was calculated for each of the depth data points Equation 4 was then rearranged to produce the equation:

$$h = \operatorname{arctanh}\left(\frac{2\pi L}{gT^2}\right)\left(\frac{L}{2\pi}\right) \tag{12}$$

to estimate the depth for each location. Depth was estimated for twenty eight points outside the surf zone off the coast of Camp Pendleton. The points where the depth was estimated corresponds to the midpoint between the pixel coordinate associated with the wave crest in image P007 and the pixel coordinate associated with the wave crest in image P009 as indicated by the green triangle in Figure 29. The estimated depths for each of these points was compared to the ground truth data as determined from the USGS DEM sd10 in ENVI. This was accomplished by first geographically linking the USGS DEM sd10 image to both images P007 and P009 in ENVI. The depth data point was located on image P007 with the Pixel Locator tool in ENVI by the pixel coordinates associated with each depth data point. Since the two images were geographically linked the locator on the USGS image located the corresponding geographical point on the

USGS image and the ground truth depth was determined from the data field of the Cursor Location/Value tool associated with the USGS image in ENVI as shown in Figure 30.

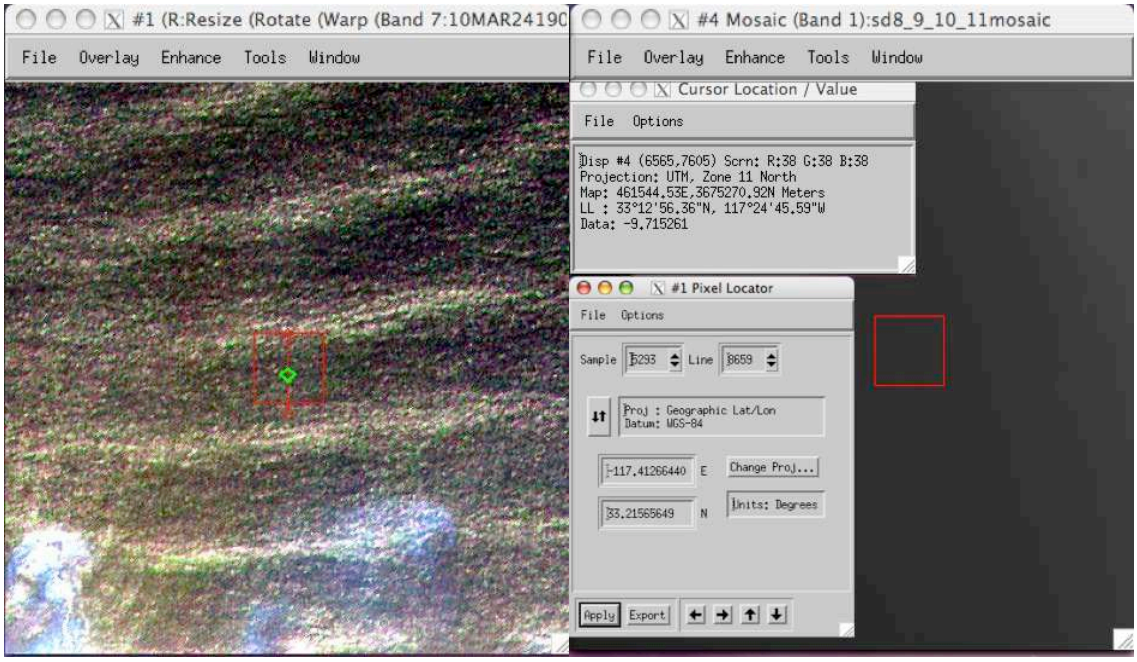

Figure 30. Ground Truth determination from USGS DEM for outside the surf zone

The estimated depths were plotted against the ground truth depths for each of the twenty eight depth data points to determine the accuracy of the wave celerity method outside the surf zone as shown in Figure 31.

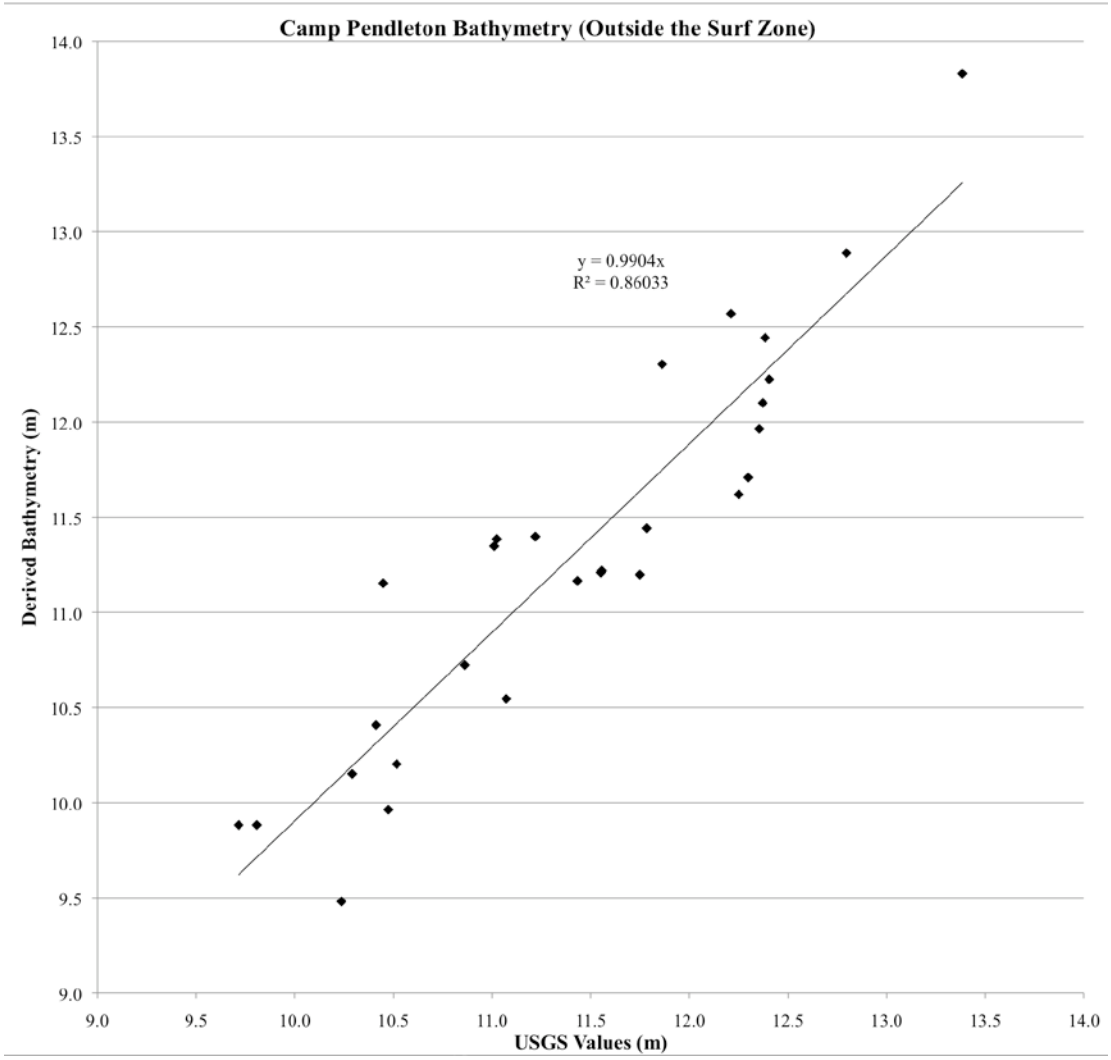

Figure 31. Plot of estimated depth versus ground truth depth outside the surf zone

Figure 31 shows that on average the wave celerity method outside the surf zone reflected less than a one percent error based on the equation for the best fit curve for the twenty eight depth data points with a coefficient of determination (R^2) of 0.86. There is again a plus or minus ten percent uncertainty in the estimated depth associated with the location measurement error of plus or minus one pixel (2.4 m). This model is much more accurate than the one determined for the surf zone because as discussed in Chapter II there is no need to account for wave height in this zone and the linear theory still holds true. The R^2 value of 0.86 says that the regression line is a near perfect fit to the data and that it is a good representative model. All estimated depths were within plus or minus one meter of ground truth and most were within plus or minus a half meter of ground truth. Table 5 in Appendix contains the specific results for each of the depth data points.

VI. SUMMARY

WorldView-2 multispectral imagery of the coastal area near Camp Pendleton, California was used to determine ocean depth for both in the surf zone and outside the surf zone by the wave celerity method and applying the linear dispersion relationship for surface gravity waves. The high spatial resolution provided by the multispectral satellite imagery was more than sufficient to resolve the waves. The high retargeting agility provided by WorldView-2 allowed for multiple images to be taken in rapid succession of the same area which in turned allowed for wave celerity to be accurately determined. The eight bands comprising the multispectral imagery provided for the removal of image contamination as well as increased degrees of freedom, further improving the image quality for performing measurements. The images were co-registered, rotated, resized and principal component transforms performed in ENVI to provide an accurate baseline of images to conduct measurements and extract data.

Principal component four was found to resolve the wave crest in the surf zone. Using the principal component four image from both images P007 and P009 a change detection image was created with an RGB image where principal component four for image P007 was represented by red and green and principal component four for image P009 was represented by blue. This produced a single image containing both spatial and temporal information where waves moved from blue to yellow in the time between images. This allowed for the accurate measurement of distance traveled by the wave between the two images from which wave celerity was calculated. The linear dispersion relationship for surface gravity waves was then applied to estimate the depth in the surf zone. This method reflected a five percent over estimation of depth on average in the surf zone, however, there were errors up to fifty percent in some individual estimates. This is a result of the fact that the linear theory begins to breakdown in the surf zone and wave height must be accounted for or an over estimation of depth can be expected as observed here.

None of the principal components clearly resolved the wave crest outside the surf zone as principal component four did in the surf zone; therefore, a change detection

image could not be created for outside the surf zone. Wave celerity for outside the surf zone was determined by geographically linking images P007 and P009 in ENVI then determining the location of the corresponding wave crest from image P009 in image P007. The distance from the wave crest in image P007 to the wave crest in image P009 was accurately measured by the ENVI measurement tool and wave celerity calculated. The linear dispersion relationship for surface gravity waves was then applied, as with the surf zone data, to estimate the depth in the region outside the surf zone. This method reflected less than a one percent error on average outside the surf zone with no more than a seven percent error for any individual estimate.

VII. CONCLUSION

Nearshore subaqueous beach profile was accurately determined both in the surf zone and outside the surf zone from WorldView-2 multispectral imagery of the coastal area near Camp Pendleton, California by the wave celerity method and applying the linear dispersion relationship for surface gravity waves. The estimated depths for each of the depth data points compared favorably with the ground truth bathymetry as determined from the USGS DEM of the same area and were more than sufficiently accurate for the purposes of IPE, especially in the region outside the surf zone. This method resulted in larger discrepancies from ground truth in the surf zone due to the fact that the linear theory begins to break down at this point, however the results were still within one meter of ground truth and in most instances were within a half meter. The results in the surf zone are sufficiently accurate at these shallow depths for the purposes of IPE in support of amphibious operations, HADR, and mine warfare planning operations.

The wave period method was determined to not be a viable method for determining nearshore bathymetry from space. This conclusion was drawn based on the fact that due to the wave dispersion process it cannot be assumed that the deep water wave period observed in an image is the same deep water period for the wave group in the shallow water or surf zones.

This study demonstrates that determining nearshore bathymetry from space by the wave celerity method is a viable solution for determining nearshore bathymetry of hostile or denied areas. Based on this proof of concept additional work needs to be done in order to automate the process so that it can be delivered to the fleet as an operational tool. Future work should include research and development of algorithms that can automatically conduct exhaustive depth computations from multiple images by accurately determining either the wave celerity or wave number for an extensive number of depth data points common to all images. From these computations a subaqueous beach profile should be created that can be used by the fleet for IPE in support of amphibious operations, HADR, and mine warfare planning.

THIS PAGE INTENTIONALLY LEFT BLANK

APPENDIX

Table 5. Data table for depth data points outside of the surf zone

pixel x-coordinate	pixel y-coordinate	distance wave travels [m]	wave phase speed [m/s]	water depth (estimate) [m]	water depth (exact equation) [m]	Ground Truth [m]	Deviation [m]	Percent Error
9332	8543	106.4600	9.8574	9.90847	11.34735	11.01	0.34	3.06
9332	8458	105.9382	9.8091	9.81158	11.21848	11.55	-0.34	2.91
9332	8352	109.4227	10.1318	10.46764	12.10027	12.37	-0.27	2.19
9332	8625	102.5471	9.4951	9.19349	10.40699	10.41	-0.01	0.05
9422	8344	107.8974	9.9905	10.17784	11.70808	12.30	-0.59	4.80
9422	8430	105.8534	9.8013	9.79588	11.19764	11.75	-0.55	4.70
9422	8525	106.6637	9.8763	9.94643	11.39796	11.22	0.18	1.58
9422	8615	105.6711	9.7844	9.76217	11.15293	10.45	0.70	6.75
9271	8374	111.1964	10.2960	10.80974	12.56889	12.21	0.36	2.94
9271	8473	105.8974	9.8053	9.80403	11.20845	11.55	-0.34	2.96
9271	8559	103.1384	9.5499	9.29982	10.54530	11.07	-0.53	4.76
9271	8635	101.6637	9.4133	9.03578	10.20279	10.52	-0.31	2.98
9471	8329	110.7227	10.2521	10.71784	12.44238	12.38	0.06	0.47
9471	8419	110.1964	10.2034	10.61619	12.30299	11.86	0.44	3.72
9471	8511	103.8914	9.6196	9.43611	10.72337	10.86	-0.14	1.27
9471	8598	101.4374	9.3924	8.99560	10.15094	10.29	-0.14	1.37
9072	8235	115.7222	10.7150	11.70758	13.82935	13.38	0.45	3.33
9072	8330	112.3716	10.4048	11.03944	12.88705	12.80	0.09	0.71
9072	8422	109.8974	10.1757	10.55866	12.22434	12.40	-0.18	1.46
5120	8366	107.5471	9.9581	10.11186	11.61939	12.25	-0.63	5.15
5120	8443	105.7222	9.7891	9.77161	11.16545	11.43	-0.27	2.33
5120	8525	100.6126	9.3160	8.84990	9.96357	10.47	-0.51	4.87
5120	8640	100.2550	9.2829	8.78711	9.88310	9.81	0.08	0.78
5293	8317	108.8974	10.0831	10.36738	11.96409	12.35	-0.39	3.15
5293	8402	106.8388	9.8925	9.97911	11.44160	11.78	-0.34	2.90
5293	8491	106.6126	9.8716	9.93690	11.38525	11.02	0.36	3.29
5293	8579	98.4374	9.1146	8.47138	9.48115	10.24	-0.75	7.37
5293	8659	100.2550	9.2829	8.78711	9.88310	9.72	0.17	1.73

Table 6. Data table for surf zone depth data points

pixel x-coordinate	pixel y-coordinate	distance wave travels [m]	wave phase speed [m/s]	water depth (estimate) [m]	water depth (exact equation) [m]	Ground Truth [m]	Deviation [m]	Percent Error
9070	9037	61.6861	5.7117	3.32666	3.46354	2.51	0.96	38.18
9036	9043	58.4107	5.4084	2.98276	3.09195	2.48	0.61	24.82
8638	9049	53.2423	4.9299	2.47826	2.55279	2.46	0.10	3.97
9055	9039	57.7970	5.3516	2.92041	3.02493	2.40	0.63	26.09
9062	9039	60.2282	5.5767	3.17127	3.29522	2.34	0.95	40.57
8601	9049	54.6074	5.0563	2.60697	2.68968	2.29	0.40	17.63
9015	9048	50.5837	4.6837	2.23694	2.29733	2.26	0.04	1.71
9003	9050	47.9293	4.4379	2.00833	2.05677	2.23	-0.17	7.71
8911	9062	50.2137	4.6494	2.20434	2.26294	2.22	0.04	1.85
8598	9049	54.6858	5.0635	2.61447	2.69766	2.19	0.51	23.34
8598	9049	51.4961	4.7682	2.31837	2.38335	2.19	0.20	8.97
8802	9064	44.1971	4.0923	1.70774	1.74253	2.17	-0.43	19.70
8806	9064	40.4041	3.7411	1.42720	1.45135	2.15	-0.70	32.43
9452	9076	44.7398	4.1426	1.74993	1.78650	2.14	-0.35	16.40
8817	9065	42.8392	3.9666	1.60441	1.63505	2.12	-0.48	22.73
8856	9062	49.6713	4.5992	2.15697	2.21303	2.12	0.10	4.63
9829	9083	49.3013	4.5649	2.12496	2.17932	2.11	0.07	3.53
9667	9069	58.3282	5.4008	2.97434	3.08289	2.10	0.98	46.80
8757	9068	51.8703	4.8028	2.35218	2.41913	2.09	0.32	15.49
8934	9059	46.5573	4.3109	1.89500	1.93802	2.09	-0.15	7.12
8936	9059	47.0169	4.3534	1.93260	1.97737	2.07	-0.09	4.41
8854	9062	49.3013	4.5649	2.12496	2.17932	2.06	0.12	5.68
9414	9077	43.3746	4.0162	1.64477	1.67700	2.06	-0.38	18.64
8899	9063	51.1188	4.7332	2.28452	2.34757	2.06	0.29	13.91
9215	9057	49.7541	4.6069	2.16417	2.22061	2.05	0.17	8.32
9346	9073	47.0169	4.3534	1.93260	1.97737	2.04	-0.07	3.28
8940	9059	46.9413	4.3464	1.92639	1.97087	2.03	-0.06	3.04
8896	9063	51.1188	4.7332	2.28452	2.34757	2.03	0.32	15.61
8959	9057	49.6713	4.5992	2.15697	2.21303	2.02	0.19	9.56
9181	9064	47.3156	4.3811	1.95723	2.00318	1.97	0.03	1.48
8971	9056	51.0364	4.7256	2.27716	2.33980	1.95	0.39	19.90
9155	9070	42.0026	3.8891	1.54236	1.57064	1.93	-0.36	18.69
8885	9064	51.0364	4.7256	2.27716	2.33980	1.91	0.43	22.47
9145	9072	41.8417	3.8742	1.53057	1.55841	1.87	-0.31	16.68
9135	9074	43.7444	4.0504	1.67293	1.70630	1.84	-0.14	7.41
8428	9053	46.4816	4.3039	1.88884	1.93157	1.84	0.09	5.17
9296	9085	41.9268	3.8821	1.53680	1.56487	1.80	-0.24	13.10
8556	9050	41.4671	3.8396	1.50328	1.53012	1.78	-0.25	14.11
8555	9050	38.7371	3.5868	1.31186	1.33222	1.75	-0.42	23.81
9536	9094	35.0101	3.2417	1.07157	1.08508	1.55	-0.46	29.77
9265	9092	43.5931	4.0364	1.66138	1.69428	1.45	0.25	17.25
8721	9087	39.3616	3.6446	1.35450	1.37622	1.32	0.06	4.19
8709	9087	42.3795	3.9240	1.57017	1.59949	1.27	0.33	26.38
9253	9096	45.5692	4.2194	1.81542	1.85483	1.24	0.62	49.76
8675	9090	37.8247	3.5023	1.25079	1.26927	1.19	0.08	7.04
9622	9108	30.6166	2.8349	0.81950	0.82736	1.18	-0.36	30.12
8640	9090	35.6307	3.2991	1.10990	1.12440	1.16	-0.04	3.20
8672	9091	36.8346	3.4106	1.18617	1.20276	1.13	0.07	6.13
8630	9092	34.8081	3.2230	1.05924	1.07244	1.08	0.00	0.41
9218	9102	44.1971	4.0923	1.70774	1.74253	1.02	0.73	71.60
8790	9104	34.6278	3.2063	1.04830	1.06122	0.85	0.21	24.65

LIST OF REFERENCES

Abileah, R., & Trizna, D. B. (2010). Shallow water bathymetry with an incoherent X-band radar using small (smaller) space-time image cubes. Paper presented at the *Geoscience and Remote Sensing Symposium (IGARSS), 2010 IEEE International,* 4330–4333. Abileah, R. (2006). *Mapping shallow water depth from satellite*. Paper presented at the *ASPRS 2006 Annual Conference,* Reno, Nevada.

Barnard, P. L., & Hoover, D. (2010). A seamless, high-resolution, coastal digital elevation model (DEM) for Southern California. *U.S.Geological Survey Data Series,* 8. Retrieved from http://search.proquest.com/docview/742920456?accountid=12702; http://pubs.usgs.gov/ds/487/

Bell, P. S. (1999). Shallow water bathymetry derived from an analysis of X-band marine radar images of waves. *Coastal Engineering, 37*(3-4), 513–527. doi: 10.1016/S0378-3839(99)00041-1

Caruthers, J. W., Arnone, R. A., Howard, W., Haney, C., & Durham, D., L. (1985). *Water Depth Determination Using Wave Refraction Analysis of Aerial Photography.* (NORDA No. 110). NSTL, Mississippi: Naval Ocean Research and Development Activity.

Corucci, L., Masini, A., & Cococcioni, M. (2011). *Approaching bathymetry estimation from high resolution multispectral satellite images using a neuro-fuzzy technique* SPIE. doi:10.1117/1.3569125

DigitalGlobe | DigitalGlobe: Worldview-2 Satellite - 46cm Resolution Retrieved 8/19/2011, 2011, from http://www.digitalglobe.com/index.php/88/WorldView-2

DigitalGlobe, I.*DigitalGlobe Core Imagery Products Guide.* Unpublished manuscript. Retrieved 8/21/2011, from http://www.digitalglobe.com/file.php/811/DigitalGlobe_Core_Imagery_Products_Guide.pdf

DigitalGlobe, I. (2010). *Whitepaper: The benefits of the 8 spectral bands of worldview-2.* Unpublished manuscript. Retrieved 8/19/2011, from http://www.digitalglobe.com/downloads/spacecraft/WorldView-2_8-Band_Applications_Whitepaper.pdfhttp://www.digitalglobe.com/downloads/spacecraft/WorldView-2_8-Band_Applications_Whitepaper.pdf

DigitalGlobe, I. (2011). *DigitalGlobe constellation - Worldview-2 imaging satellite.* Unpublished manuscript. Retrieved 8/19/2011, from http://www.digitalglobe.com/downloads/spacecraft/WorldView2-DS-WV2.pdf

ENVI, IDL, & Industry Brochures from ITT Visual Information Solutions Retrieved 8/21/2011, 2011, from http://www.ittvis.com/language/en-U.S./ProductsServices/ProductBrochures.aspx

Gao, J. (2009). Bathymetric mapping by means of remote sensing: methods, accuracy and limitations. *Progress in Physical Geography, 33*(1), 103–116. doi:10.1177/0309133309105657

Holland, K. T. (2001). Correction to "application of the linear dispersion relation with respect to depth inversion and remotely sensed imagery." *Geoscience and Remote Sensing, IEEE Transactions on, 39*(10), 2319–2319.

Komar, P. D. (1998). *Beach processes and sedimentation* (2nd ed.). Upper Saddle River, N.J: Prentice Hall.

McCarthy, B. L., & Naval Postgraduate School (U.S.). (2010). *Coastal bathymetry using 8-color multispectral satellite observation of wave motion [electronic resource]*. Monterey, CA: Naval Postgraduate School. Retrieved from http://edocs.nps.edu/npspubs/scholarly/theses/2010/Sep/10Sep%5FMcCarthy.pdf (18.07 MB); http://handle.dtic.mil/100.2/ADA531460

Olsen, R. C. (2007). *Remote sensing from air and space*. Bellingham, WA: SPIE Press.

OPNAV N2/N6. (2010). *Navy Space Capability Needs.* (OPNAV N2/N6 Memo 5910 No. 10S150054). Arlington, VA: OPNAV.

Plant, N. G., Holland, K. T., & Haller, M. C. (2008). Ocean Wavenumber Estimation From Wave-Resolving Time Series Imagery. *Geoscience and Remote Sensing, IEEE Transactions on, 46*(9), 2644–2658.

Stockdon, H. F., & Holman, R. A. (2000). Estimation of wave phase speed and nearshore bathymetry from video imagery. *Journal of Geophysical Research, Oceans, 105*, 22015–22033. Retrieved from http://search.proquest.com/docview/17718325?accountid=12702

Williams, W. W. (1947). The determination of gradients on enemy-held beaches. *The Geographical Journal, 109*(1/3), 76–90.

INITIAL DISTRIBUTION LIST

1. Defense Technical Information Center
   Ft. Belvoir, Virginia

2. Dudley Knox Library
   Naval Postgraduate School
   Monterey, California

3. Dr. Richard C. Olsen
   Remote Sensing Center at the Naval Postgraduate School
   Monterey, California

4. Dr. Jamie MacMahan
   Naval Postgraduate School
   Monterey, California